OPEN ACCESS

Original research

Enolase represents a metabolic checkpoint controlling the differential exhaustion programmes of hepatitis virus-specific CD8$^+$ T cells

Frances Winkler,[1,2] Anna V Hipp,[1] Carlos Ramirez,[3] Bianca Martin,[1] Matteo Villa,[4] Emilia Neuwirt,[5,6] Oliver Gorka,[5] Jeroen Aerssens,[7] Susanne E Johansson,[7] Nisha Rana,[1] Sian Llewellyn-Lacey,[8] David A Price ,[8,9] Marcus Panning,[10] Olaf Groß,[5,6] Erika L Pearce,[11] Carl M Hermann,[3] Kathrin Schumann,[12] Luciana Hannibal,[13] Christoph Neumann-Haefelin,[1] Tobias Boettler ,[1] Percy Knolle,[14,15] Maike Hofmann ,[1] Dirk Wohlleber,[15] Robert Thimme ,[1] Bertram Bengsch [1,6,16]

► Additional supplemental material is published online only. To view, please visit the journal online (http://dx.doi.org/10.1136/gutjnl-2022-328734).

For numbered affiliations see end of article.

Correspondence to
Professor Bertram Bengsch, Clinic for Internal Medicine II, Freiburg University Medical Center, Faculty of Medicine, University of Freiburg, Freiburg im Breisgau 79106, Germany; bertram.bengsch@uniklinik-freiburg.de

Received 19 September 2022
Accepted 20 June 2023
Published Online First
4 August 2023

To cite: Winkler F, Hipp AV, Ramirez C, *et al*. *Gut* 2023;**72**:1971–1984.

ABSTRACT

Objective Exhausted T cells with limited effector function are enriched in chronic hepatitis B and C virus (HBV and HCV) infection. Metabolic regulation contributes to exhaustion, but it remains unclear how metabolism relates to different exhaustion states, is impacted by antiviral therapy, and if metabolic checkpoints regulate dysfunction.

Design Metabolic state, exhaustion and transcriptome of virus-specific CD8$^+$ T cells from chronic HBV-infected (n=31) and HCV-infected patients (n=52) were determined *ex vivo* and during direct-acting antiviral (DAA) therapy. Metabolic flux and metabolic checkpoints were tested *in vitro*. Intrahepatic virus-specific CD8$^+$ T cells were analysed by scRNA-Seq in a HBV-replicating murine *in vivo* model of acute and chronic infection.

Results HBV-specific (core$_{18\text{-}27}$, polymerase$_{455\text{-}463}$) and HCV-specific (NS3$_{1073\text{-}1081}$, NS3$_{1406\text{-}1415}$, NS5B$_{2594\text{-}2602}$) CD8$^+$ T cell responses exhibit heterogeneous metabolic profiles connected to their exhaustion states. The metabolic state was connected to the exhaustion profile rather than the aetiology of infection. Mitochondrial impairment despite intact glucose uptake was prominent in severely exhausted T cells linked to elevated liver inflammation in chronic HCV infection and in HBV polymerase$_{455\text{-}463}$ -specific CD8$^+$ T cell responses. In contrast, relative metabolic fitness was observed in HBeAg-negative HBV infection in HBV core$_{18\text{-}27}$-specific responses. DAA therapy partially improved mitochondrial programmes in severely exhausted HCV-specific T cells and enriched metabolically fit precursors. We identified enolase as a metabolic checkpoint in exhausted T cells. Metabolic bypassing improved glycolysis and T cell effector function. Similarly, enolase deficiency was observed in intrahepatic HBV-specific CD8$^+$ T cells in a murine model of chronic infection.

Conclusion Metabolism of HBV-specific and HCV-specific T cells is strongly connected to their exhaustion severity. Our results highlight enolase as metabolic regulator of severely exhausted T cells. They connect differential bioenergetic fitness with distinct exhaustion subtypes and varying liver disease, with implications for therapeutic strategies.

WHAT IS ALREADY KNOWN ON THIS TOPIC

⇒ Accumulation of exhausted CD8$^+$ T cells in patients with chronic hepatitis B and C virus (HBV and HCV) infection contributes to the failure to clear viral infection.
⇒ These exhausted T cells lack sufficient antiviral function but the mechanisms behind this dysfunction are unclear.

WHAT THIS STUDY ADDS

⇒ HBV-specific and HCV-specific CD8$^+$ T cells exhibit distinct metabolic profiles that correlate with severity of exhaustion.
⇒ Severe mitochondrial depolarisation despite high glucose uptake is present in severely exhausted virus-specific CD8$^+$ T cells.
⇒ HBV polymerase$_{455\text{-}463}$-specific CD8$^+$ T cells in cHBV infection display more severe exhaustion and mitochondrial dysfunction that correlates with quantitative HB surface antigen levels in contrast to HBV core$_{18\text{-}27}$-specific CD8$^+$ T cells.
⇒ Enolase is a metabolic checkpoint limiting glycolytic flux in HBV-specific and HCV-specific CD8$^+$ T cells.
⇒ Effector function of enolase-inhibited CD8$^+$ T cells is boosted by pyruvate supplementation.

HOW THIS STUDY MIGHT AFFECT RESEARCH, PRACTICE OR POLICY

⇒ We identified the glycolytic enzyme enolase as a metabolic checkpoint that can restrict mitochondrial metabolism and effector function of HBV-specific and HCV-specific CD8$^+$ T cells.
⇒ This knowledge points to interventions to enhance or bypass enolase activity in order to boost antiviral responses in chronic infection.
⇒ Our data suggest that the exhaustion and metabolic state of HBV polymerase$_{455\text{-}463}$-specific CD8$^+$ T cells may act as correlates of differential antigen recognition in cHBV infection which should be further investigated.

INTRODUCTION

Exhausted virus-specific CD8$^+$ T cells (T_{EX}) with limited effector function accumulate in patients with chronic hepatitis B and C virus infection (cHBV/cHCV).[1–4] These exhausted T cells are characterised by increased PD-1 expression and other coinhibitory receptors and profound alterations in transcriptional programmes.[2 5 6] Recent reports highlighted substantial heterogeneity among exhausted HBV-specific and HCV-specific CD8$^+$ T cells, including early differentiated PD-1$^+$CD127$^+$ precursors of exhausted T cells with partial memory-like characteristics and more severely exhausted PD-1^{hi}CD127$^-$ T cells.[5 7–10] Interestingly, many cellular alterations of exhausted virus-specific CD8$^+$ T cells persist even after antiviral therapy.[7 10–13] However, the precise mechanisms determining these exhausted T cell programmes remain poorly defined.

T cell energy metabolism and effector T cell function are tightly interconnected. Specific roles of glycolytic enzymes in T cell activation and cytokine production have been described, such as glyceraldehyde phosphate dehydrogenase (GAPDH),[14 15] pyruvate dehydrogenase kinase 1 (PDHK1)[16] or the glycolytic metabolite phosphoenolpyruvate (PEP).[17] Conversely, regulation of the metabolic flux may explain limited T cell function. Indeed, bioenergetic regulation downstream of inhibitory receptor signalling was identified as a major hallmark of exhausted T cells in the murine lymphocytic choriomeningitis virus (LCMV) model of chronic viral infection.[18] This bioenergetic regulation affected glycolysis and resulted in a significant disorganisation of mitochondrial organelles with alterations in ultrastructure, membrane depolarisation and production of reactive oxygen species (ROS).[17–19] Investigations of the metabolic properties of HBV-specific and HCV-specific CD8$^+$ T cells identified related metabolic dysregulation. HBV-specific CD8$^+$ T cells analysed *in vitro* were highly dependent on glycolysis, and unable to switch efficiently to oxidative phosphorylation (OXPHOS) in settings of glucose restriction.[20] Fisicaro *et al.* identified that significant downregulation of mitochondrial function is connected to ROS production in exhausted HBV-specific CD8$^+$ T cells - comparable to the findings in LCMV infection.[21] HBV-specific CD8$^+$ T cells targeting different epitopes, such as HBV core$_{18\text{-}27}$-specific or polymerase$_{455\text{-}463}$-specific responses differ in their exhaustion phenotype[9] but their metabolic properties are unknown. Mitochondrial function was also investigated in HCV-specific CD8$^+$ T cells and during direct-acting antiviral (DAA) therapy. While one study reported limited changes in mitochondrial function of HCV-specific CD8$^+$ T cells after DAA therapy and HCV clearance,[11] another study observed a reduction of cells with depolarised mitochondria.[22] However, currently, it remains unclear whether there are differences in the metabolic regulation of HBV-specific and HCV-specific CD8$^+$ T cells, how these relate to the severity of exhaustion programmes, whether they change during antiviral therapy, and if specific glycolytic checkpoints are involved.

To address these important questions, we performed a detailed analysis of the metabolic profiles of HBV-specific and HCV-specific CD8$^+$ T cells and their exhaustion states. We observed major differences in the exhaustion and metabolic programmes of HBV-specific and HCV-specific CD8$^+$ T cells. HCV-specific responses were enriched for more severe exhaustion phenotypes and connected to more pronounced mitochondrial impairment despite high glucose uptake. However, a similar mitochondrial impairment was observed in HBV polymerase$_{455\text{-}463}$-specific CD8$^+$ T cells but not in HBV core$_{18\text{-}27}$-specific CD8$^+$ T cells during HBeAg-negative infection. These differences were connected to more severe exhaustion and in cHCV to a higher level of liver inflammation. In HBV infection, a correlation between HBV polymerase$_{455\text{-}463}$-specific metabolism and quantitative HB surface antigen (qHBsAg) levels was observed. Antigen removal *in vivo* during DAA therapy partially improved the metabolism of the more severely exhausted T cell subset. Enolase was identified as a metabolic checkpoint. Its reduced expression in severely exhausted CD8$^+$ T cells is involved in regulation of the glycolytic flux, contributing to metabolic dysfunction and reduced antiviral effector function. Bypassing this metabolic bottleneck reinvigorated effector function of virus-specific CD8$^+$ T cells. Enolase deficiency was a conserved feature of severely exhausted murine intrahepatic HBV-specific CD8$^+$ T cells in chronic but not acute infection. Together, these data highlight differential metabolic programming of virus-specific CD8$^+$ T cells in different exhausted T cell subsets in viral hepatitis and highlight a novel metabolic checkpoint.

METHODS

Study cohort

Patient details are summarised in online supplemental tables 1 and 2.

Peptides, tetramers and antibodies

HLA-A*02:01-restricted monomers of immunodominant epitopes for HBV (HLA-A*02:01/core$_{18\text{-}27}$: FLPSDFFPSV; HLA-A*02:01/polymerase$_{455\text{-}463}$: GLSRYVARL), HCV (HLA-A*02:01/NS3$_{1073\text{-}1081}$: CINGVCWTV; HLA-A*02:01/NS3$_{1406\text{-}1415}$: KLVALGINAV; HLA-A*02:01/NS5B$_{2594\text{-}2602}$: ALYDVVSKL), EBV (HLA-A*02:01/BMLF1$_{280\text{-}288}$: GLCTLVAML), CMV (HLA-A*02:01/pp65$_{495\text{-}503}$: NLVPMVATV) and FLU (HLA-A*02:01/M1$_{58\text{-}66}$: GILGFVFTL) were synthesised and conjugated with allophycocyanin (APC)-labelled or phycoerythin (PE)-labelled Streptavidin (Agilent) in a molar 4:1 ratio. Antibodies used are listed in online supplemental table 3.

Statistics

Statistical analyses were performed using GraphPad Prism V.9 (GraphPad Prism Software, USA). Normal (Gaussian) distribution of the data was tested using the D'Agostino and Pearson test. Normally distributed data sets (alpha=0.05) were analysed using parametric statistical tests and not normally distributed data sets were analysed using non-parametric statistics. For the comparison of two groups (un)paired t-test, Mann-Whitney U test or Wilcoxon test was used. The comparison of more than two groups was statistically tested using analysis of variance (ANOVA), Kruskal-Wallis test or Friedman test. Tests used in figures 1–7 and online supplemental figures 1–5 were: Unpaired t-test: figure 1C,F and G (centre and right) and online supplemental figure 3F (MTDR, MTDR/MTG) and online supplemental figure 3G (left). Paired t-test: figure 3A (right), figure 4E, figure 6C, online supplemental figure 4H (MTDR/MTG), online supplemental figure 4J, online supplemental figure 5H (left) and I. Wilcoxon test: figure 3A (left), figure 3B,C, figure 4A–C and G–K, figure 6G,I and K, online supplemental figure 4H (MTG, MTDR, MTG$^+$MTDR$^-$), online supplemental figure 4I,K-M and online supplemental figure 5H (right). Mann-Whitney test: figure 1A,B,D,E and G (left), figure 5B–D, figure 7H,I, online supplemental figure 1C–E, online supplemental figure 2A,B, online supplemental figure 3F (MTG, MitoSox), online supplemental figure 3G (right) and online supplemental figure 3H. ANOVA: figure 6L (right), online supplemental figure 5B,E. Kruskal-Wallis test: figure 2D–I, figure 5A, figure 6B, online supplemental figure 1G,H and online supplemental figure 4B. Friedman test: figure 6H,J and L (left) and online supplemental figure 5C,F. Pearson correlation: online supplemental figure 2G (right). Spearman correlation: figure 3D, figure 4D,F, figure 5E–F, figure 6D–F, online supplemental figure 2C–F, G (left),

H–L, online supplemental figure 3B–D and online supplemental figure 4C–G. Statistical tests used are depicted in the figure legends (p*>0.05; p**>0.01; p***>0.001; p****>0.0001). Please see online supplemental methods for additional methods used.

RESULTS

Heterogeneity of exhaustion profiles indicates bias towards severe exhaustion of HCV-specific CD8+ T cells

We set out to understand how metabolic profiles of HBV-specific and HCV-specific CD8+ T cell responses in chronic infection are connected to their exhaustion profiles. Virus-specific CD8+ T cells were identified by *ex vivo* tetramer staining which revealed a higher frequency of HBV $core_{18-27}$-specific compared with HCV $NS3_{1073-1081}$-specific, $NS3_{1406-1415}$-specific and $NS5B_{2594-2602}$-specific CD8+ T cells (figure 1A). HCV-infected patients had more variable liver inflammation with more severe hepatitis identified by transaminase elevation compared with our cohort of HBeAg-negative cHBV patients, as expected (online supplemental tables 1 and 2).[6 9] We characterised the expression of exhaustion markers that inform about early differentiated 'progenitor' exhausted T cells with homeostatic properties and more severely exhausted T cell populations.[7 18] PD-1 expression was shared by HBV-specific and HCV-specific CD8+ T cells but expression of the interleukin 7 receptor α-chain (CD127) was significantly reduced in HCV-specific CD8+ T cells, resulting in an enrichment of the PD-1+CD127+ subset in HBV $core_{18-27}$-specific CD8+ T cells (figure 1B–D). Of note, HCV-specific CD8+ T cells also expressed higher levels of CD38, CD39 and CD57, indicating stronger activation and a more severely exhausted phenotype, while no major differences in TIGIT, CD27, CD28 and CD122 expression were observed (figure 1E–G). Together, these data indicate significant heterogeneity of the exhaustion profiles of HBV $core_{18-27}$-specific and HCV $NS3_{1073-1081}$-specific, $NS3_{1406-1415}$-specific and $NS5B_{2594-2602}$-specific CD8+ T cells in our cohort.

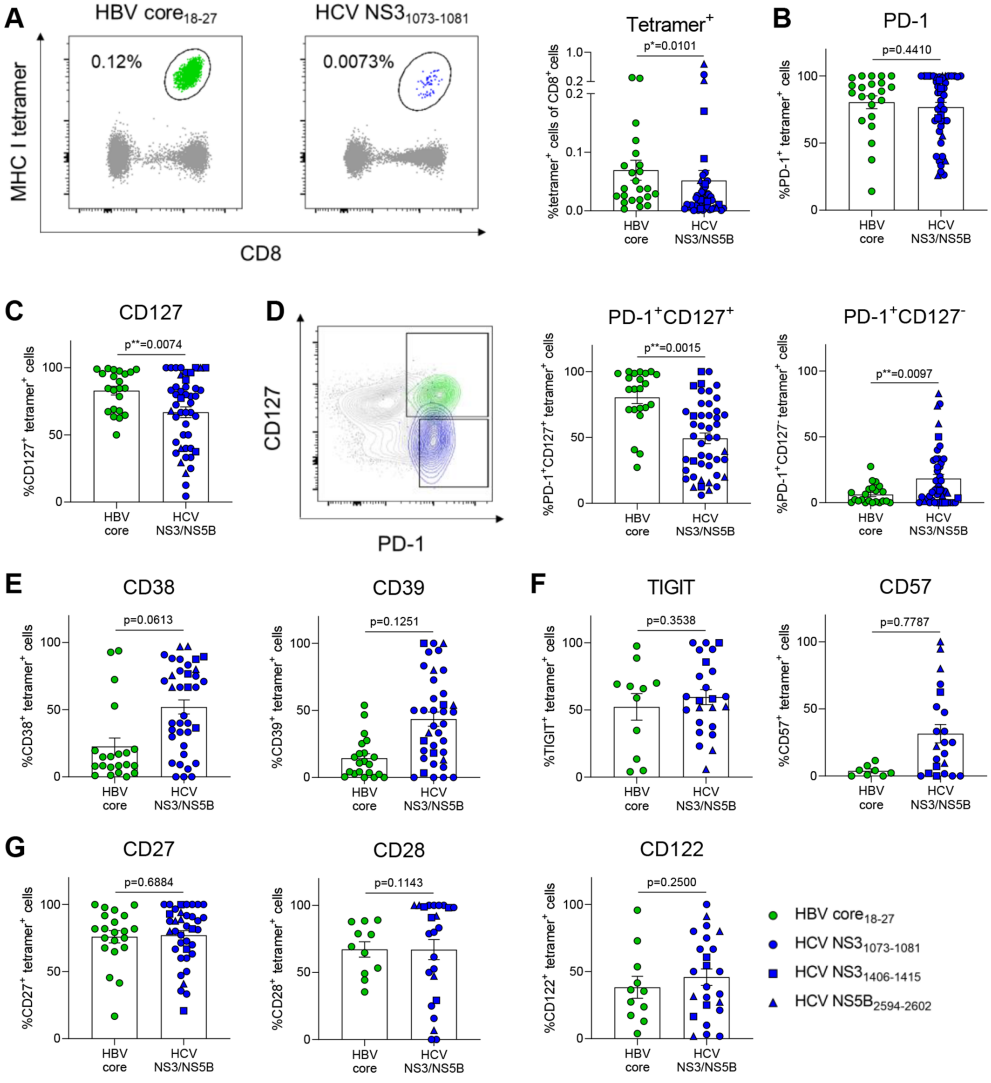

Figure 1 HCV-specific CD8+ T cells express markers associated with severe exhaustion. (A) Tetramer analysis of PBMCs from therapy-naïve cHBV and cHCV patients. Representative FACS plots of HBV $core_{18-27}$- and HCV $NS3_{1073-1081}$-specific CD8+ T cells (left). Comparison of tetramer frequencies gated on CD8+ T cells (right). Virus-specific CD8+ T cells from cHBV and cHCV patients were stained for the depicted exhaustion-associated molecules. (B, C) Frequencies of PD-1+, CD127+, (D) PD-1+CD127+, PD-1+CD127-, (E) CD38+, CD39+, (F) TIGIT+, CD57+, (G) CD27+, CD28+ and CD122+ virus-specific CD8+ T cells are indicated. HBV $core_{18-27}$ (green) and HCV $NS3_{1073-1081}$ epitopes (blue) are represented by circles. HCV $NS3_{1406-1415}$ and HCV $NS5B_{2594-2602}$ epitopes are visualised by blue squares and triangles, respectively. Mann-Whitney test was performed in (A, B), (D, E) and (G, left). Unpaired t-test was performed in (C), (F, G, centre and right). P values are indicated (p*<0.05, p**<0.01). Error bars indicate mean±SEM. cHBV, chronic hepatitis B virus; cHCV, chronic hepatitis C virus; PBMCs, peripheral blood mononuclear cells.

Hepatitis virus-specific CD8$^+$ T cells exhibit different metabolic programmes

Our exhaustion analysis indicated that the comparison of HBV core$_{18\text{-}27}$-specific CD8$^+$ T cells and HCV NS3$_{1073\text{-}1081}$-specific, NS3$_{1406\text{-}1415}$-specific and NS5B$_{2594\text{-}2602}$-specific CD8$^+$ T cells also reflected a comparison between mild and severe exhaustion programmes. The comparison of HBV-specific and HCV-specific CD8$^+$ T cell responses thus may not only reflect differences in viral aetiology but also serves as a model to study differences in T cell exhaustion programmes. To understand the metabolic profiles of virus-specific CD8$^+$ T cells in chronic HBV and HCV infection, we first performed transcriptome analysis of sorted virus-specific CD8$^+$ T cells in untreated chronic infection. Interestingly, gene set enrichment analysis (GSEA) of KEGG metabolic pathways indicated significant differences in the metabolic programmes of mildly exhausted HBV-specific compared with severely exhausted HCV-specific CD8$^+$ T cells (figure 2A). In particular, the gene sets for OXPHOS and citric acid cycle (TCA cycle) were significantly enriched in HBV-specific CD8$^+$ T cells, while expression of genes involved in glycolysis had a non-significant trend towards higher expression in HCV-specific CD8$^+$ T cells (figure 2B). These transcriptional analyses suggested differences in energy metabolism of HBV-specific and HCV-specific CD8$^+$ T cells. We thus explored the functional consequences of these altered transcriptomes and functionally interrogated T cell metabolism using metabolism-directed flow cytometry. Glucose uptake was measured using 2-NBDG assay. HBV-specific and HCV-specific CD8$^+$ T cells incorporated more 2-NBDG than naïve T cells, in line with higher bioenergetic requirements of activated antigen-specific CD8$^+$ T cells (figure 2C,D).

We next assessed the mitochondrial properties of virus-specific CD8$^+$ T cells using several mitochondrial dyes that differ in their ability to stain mitochondria depending on their membrane potential. TMRE staining as a direct correlate of $\Delta\Psi$m electronegativity was significantly higher in HBV-specific compared with HCV-specific CD8$^+$ T cells, indicating elevated mitochondrial membrane potential (figure 2E). In contrast, elevated mitochondrial mass, as indicated by MitoTracker Green (MTG) staining was observed in HCV-specific CD8$^+$ T cells despite similar total cellular uptake of the MitoTracker Deep Red (MTDR) that correlates with mass and potential (figure 2F,G). The MTDR/MTG ratio (informing about relative mitochondrial polarisation as another estimate of mitochondrial membrane potential) was reduced in HCV-specific CD8$^+$ T cells, fitting to the TMRE results (figure 2H). We also observed higher mitochondrial ROS in HBV-specific and HCV-specific CD8$^+$ T cells compared with naïve T cells, however, there was a clear enrichment of ROS in HCV-specific compared with HBV-specific CD8$^+$ T cells (figure 2I). These data inform about a pronounced alteration of mitochondrial function in HCV NS3$_{1073\text{-}1081}$-specific, NS3$_{1406\text{-}1415}$-specific and NS5B$_{2594\text{-}2602}$-specific CD8$^+$ T cells and, together, indicated significant heterogeneity in the metabolic programming of hepatitis virus-specific CD8$^+$ T cells during chronic infection.

To understand if these surrogates of mitochondrial function translate into a differential ability to respire, we performed Seahorse analysis of (n=16) *in vitro* expanded HBV-specific and HCV-specific CD8$^+$ T cell lines and control cell lines. We observed significant metabolic heterogeneity across these cell lines (online supplemental figure 1A,B). Interestingly, HBV-specific CD8$^+$ T cells had a higher spare respiratory capacity compared with HCV-specific CD8$^+$ T cell lines (online supplemental figure 1C). In glucose-starved flux assays, there was a trend towards higher glycolytic capacity in HBV-specific CD8$^+$ T cell lines (online supplemental figure 1D). The difference in the glycolytic capacity was significant in the flux analysis of non-starved cells (online supplemental figure 1E). These data suggest that a higher relative metabolic fitness of HBV-specific CD8$^+$ T cells can be observed *in vitro*, correlating to the *ex vivo* profiling. The ability of HBV-specific CD8$^+$ T cells to respond to oligomycin-mediated inhibition of ATP synthase with increased ECAR indicates higher metabolic flexibility to alternatively use glycolysis for ATP production (online supplemental figure 1F). This is in contrast to HCV-specific CD8$^+$ T cells, which in some cell lines could not increase their ECAR at all, despite effects on OCR (online supplemental figure 1G,H). In summary, these experiments illustrate significant metabolic heterogeneity in HBV-specific and HCV-specific CD8$^+$ T cells with a bias to more significant mitochondrial impairment in severely exhausted HCV-specific CD8$^+$ T cells.

The mitochondrial profile of HBV-specific and HCV-specific CD8$^+$ T cells is associated with their differential PD-1/CD127 expression

We next examined the extent to which the mitochondrial polarisation depends on the exhausted subpopulations in cHBV and cHCV infection. Analysis of mitochondrial mass, potential and polarisation between PD-1$^+$CD127$^+$ and PD-1$^+$CD127$^-$ virus-specific CD8$^+$ T cells in cHBV and cHCV infection revealed significantly reduced mitochondrial polarisation in the more exhausted PD-1$^+$CD127$^-$ subset, independent of aetiology of viral infection (figure 3A–C). In line with this observation, linear regression analysis also revealed a direct correlation of mitochondrial polarisation and the PD1/CD127 phenotype. Mitochondrial polarisation (MTDR/MTG) inversely correlated with the PD-1$^+$CD127$^-$ subset frequency, in contrast to a positive correlation with the mildly exhausted subset (PD-1$^+$CD127$^+$) in HBV-specific and HCV-specific CD8$^+$ T cells (figure 3D). These analyses demonstrate a connection of the mitochondrial polarisation with the distribution of different exhaustion subsets of HBV core$_{18\text{-}27}$-specific and HCV NS3$_{1073\text{-}1081}$-specific, NS3$_{1406\text{-}1415}$-specific and NS5B$_{2594\text{-}2602}$-specific CD8$^+$ T cells and suggest that the metabolic differences are connected to the differentiation of exhausted subsets rather than differences inherent to the different hepatitis viruses.

Antigen clearance improves mitochondrial fitness of HCV-specific CD8$^+$ T cells linked to accumulation of PD-1$^+$CD127$^+$ populations

Since we had identified severely impaired mitochondrial metabolism in exhausted HCV-specific CD8$^+$ T cells associated with a terminally exhausted phenotype (PD-1$^+$CD127$^-$) during chronic infection that is associated with high levels of antigen stimulation and liver inflammation, we sought to understand if direct-acting antiviral (DAA) therapy would reprogramme HCV-specific CD8$^+$ T cell metabolism. Previous studies had shown controversial results on a bulk virus-specific analytic level after overnight culture.[11 22] Therefore, we performed a longitudinal metabolic analysis of HCV-specific CD8$^+$ T cells *ex vivo* in cHCV patients treated with DAA therapy. Interestingly, *ex vivo* analysis identified a significant increase of virus-specific cells at week 2 after therapy initiation (figure 4A), suggesting an augmented virus-specific response, that occurred when transaminase levels significantly declined (figure 4B).

Metabolic analysis revealed an increase in the polarisation of mitochondria after 2 weeks of therapy (figure 4C). Interestingly, we observed a negative association between mitochondrial fitness and ALT levels (figure 4D). Thus, our *ex vivo* analyses indicated a metabolic response to DAA therapy. We next wondered if the improved mitochondrial fitness was associated with a change in

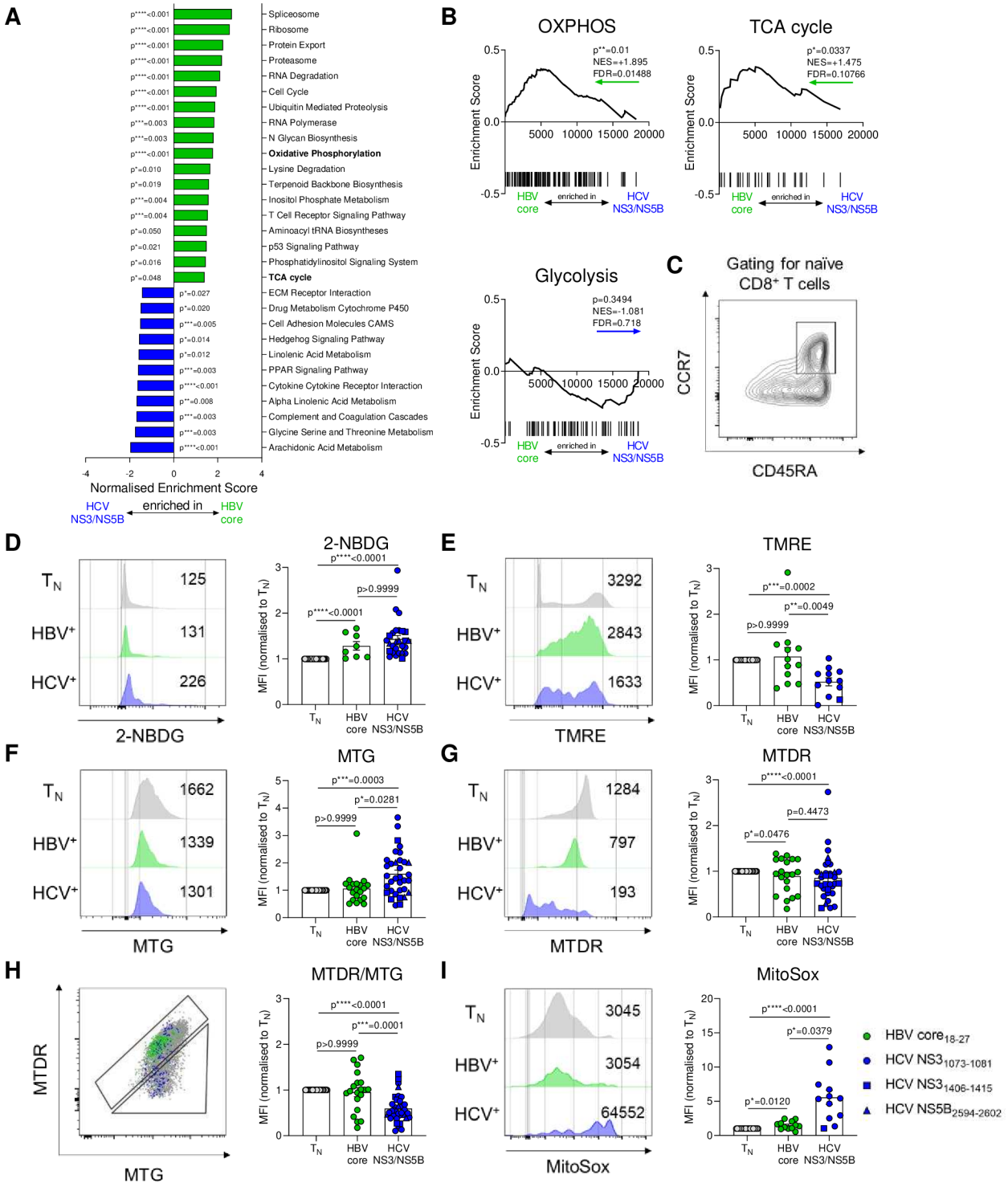

Figure 2 HBV-specific and HCV-specific CD8$^+$ T cells display different metabolic profiles. (A) Gene-set enrichment analyses (GSEA) of KEGG metabolic pathways were performed on microarray data of sorted therapy-naïve HBV-specific and HCV-specific CD8$^+$ T cells. Significant (p≤0.05) pathways were indicated. (B) GSEA plots for KEGG OXPHOS, TCA cycle and Glycolysis gene sets. Coloured arrows indicate enrichment in HBV-specific or HCV-specific CD8$^+$ T cells. Normalised enrichment scores (NES), false discovery rates (FDR) and p values are shown for GSEA analyses. (C) Naïve CD8$^+$ T cells used as normalisation control for metabolic stainings were gated as CCR7$^+$CD45RA$^+$. (D) Virus-specific CD8$^+$ T cells were analysed for metabolic features by staining for glucose uptake (2-NBDG), (E) mitochondrial membrane potential (TMRE), (F) mitochondrial mass (MTG), (G) mitochondrial mass and potential (MTDR), (H) polarisation (MTDR/MTG) and (I) mitochondrial ROS (MitoSox). Metabolic staining intensity was normalised to naïve CD8$^+$ T cells from the same sample. Exemplary histograms of metabolic stainings are shown. HBV core$_{18\text{-}27}$ (green) and HCV NS3$_{1073\text{-}1081}$ epitopes (blue) are represented by circles. HCV NS3$_{1406\text{-}1415}$ and HCV NS5B$_{2594\text{-}2602}$ epitopes are visualised by blue squares and triangles, respectively. Kruskal-Wallis test was performed in (D–I). P values are indicated (p*<0.05, p**<0.01, p***<0.005, p****<0.001). Error bars indicate mean±SEM. HBV, hepatitis B virus; HCV, hepatitis C virus; ROS, reactive oxygen species.

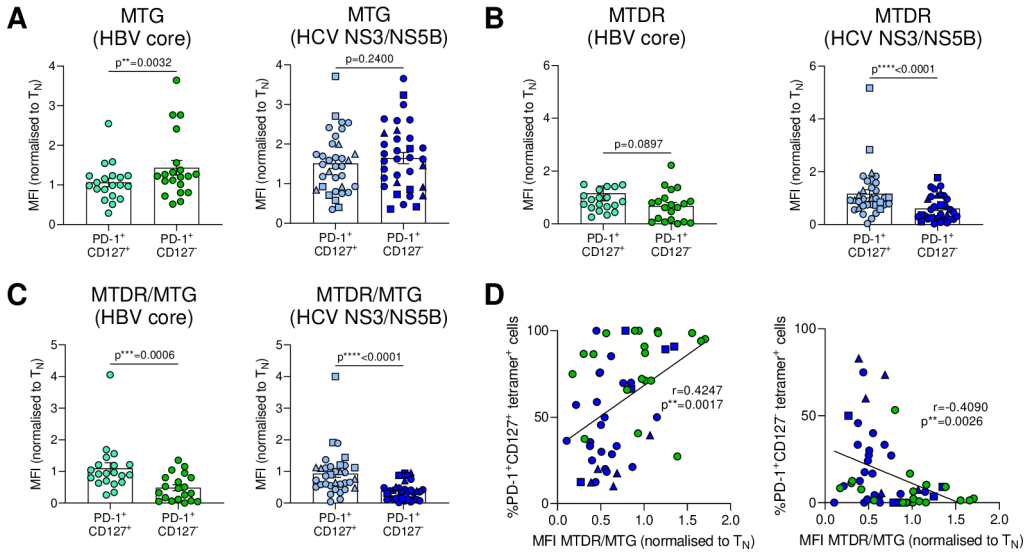

Figure 3 Severely exhausted virus-specific CD8$^+$ T cells marked by PD-1$^+$CD127$^-$ phenotype show reduced mitochondrial polarisation. (A) PD-1$^+$CD127$^+$ and PD-1$^+$CD127$^-$ subsets of HBV-specific and HCV-specific CD8$^+$ T cells were analysed *ex vivo* for mitochondrial mass (MTG), (B) mitochondrial mass and membrane potential (MTDR) and (C) mitochondrial polarisation (MTDR/MTG). (D) Correlation analyses of PD-1$^+$CD127$^+$ or PD-1$^+$CD127$^-$ virus-specific CD8$^+$ T cells and their mitochondrial polarisation are shown. Metabolic staining intensity was normalised to naïve CD8$^+$ T cells from the same sample. HBV core$_{18\text{-}27}$ (green) and HCV NS3$_{1073\text{-}1081}$ epitopes (blue) are represented by circles. HCV NS3$_{1406\text{-}1415}$ and HCV NS5B$_{2594\text{-}2602}$ epitopes are visualised by blue squares and triangles, respectively. Wilcoxon test was performed in (A, left) and (B, C). Paired t-test was performed in (A, right). Spearman r correlation analysis was performed in (D). P values are indicated (p**<0.01, p***<0.005, p****<0.001). Error bars indicate mean±SEM. HBV, hepatitis B virus; HCV, hepatitis C virus.

the distribution of exhaustion subsets. Indeed, our monitoring showed an enrichment of PD-1$^+$CD127$^+$ cells during DAA therapy (figure 4E). Clearly, the increased frequency of the PD-1$^+$CD127$^+$ subset correlated with higher mitochondrial polarisation (figure 4F). We, thus, wondered if DAA therapy augmented the metabolism in severely exhausted cells or if the increase in mitochondrial metabolism is due to an accumulation of the metabolically fit subset. We did not observe significant changes in mitochondrial metabolism in the PD-1$^+$CD127$^+$ cells during therapy (figure 4G–I). In contrast, there was an increase in polarisation in the remaining severely exhausted PD-1$^+$CD127$^-$ cells during therapy (figure 4G–I). The augmentation of mitochondrial metabolism in the severely exhausted cells compared with the PD-1$^+$CD127$^+$ subset resulted in a similar mitochondrial polarisation of the remaining PD-1$^+$CD127$^-$ cells at week 2 (figure 4J,K). In sum, our data link the enhanced metabolic fitness of HCV-specific CD8$^+$ T cells after therapy to an expansion of the PD-1$^+$CD127$^+$ population and improvement of the metabolic fitness of PD-1$^+$CD127$^-$ cells.

The metabolic profile of HBV core$_{18\text{-}27}$-specific and polymerase$_{455\text{-}463}$ -specific CD8$^+$ T cell responses significantly differs and correlates with their exhaustion phenotype

In chronic HBV infection, *ex vivo* HBV-specific CD8$^+$ tetramer responses are preferentially identified in HBeAg-negative infection.[6] Comparison of immunodominant epitope responses recently revealed phenotypic and functional differences between HBV core$_{18\text{-}27}$-specific and polymerase$_{455\text{-}463}$-specific CD8$^+$ T cells in patients despite similar low viral loads and inflammation.[9] We, thus, wondered if these responses differed in their metabolic profile. Interestingly, HBV polymerase$_{455\text{-}463}$-specific CD8$^+$ T cells had significantly reduced mitochondrial polarisation and increased mitochondrial ROS production compared with HBV core$_{18\text{-}27}$-specific CD8$^+$ T cells (figure 5A), resembling the metabolic programme enriched in severely exhausted T cells and typical for HCV infection. Consistent with our previous analysis, HBV polymerase$_{455\text{-}463}$-specific CD8$^+$ T cells had reduced frequencies of the PD1$^+$CD127$^+$ subset compared with HBV core$_{18\text{-}27}$-specific CD8$^+$ T cells (figure 5B) and higher expression of severe exhaustion-associated markers CD38, CD39, CD57 and reduced expression of CD28 (figure 5C,D). These data indicate that HBV polymerase$_{455\text{-}463}$-specific CD8$^+$ T cells have a more severe mitochondrial dysfunction that is connected to their exhaustion programme. Overall these data are in line with the connection of metabolism to exhaustion state also observed in chronic HCV infection.

Activation and metabolism of HBV polymerase$_{455\text{-}463}$-specific CD8$^+$ T cell responses correlate with qHBsAg levels

Since the differences in metabolism and exhaustion programme of HBV-specific responses could not be explained by the degree of liver inflammation, we wondered if they were connected to antigen levels. We thus determined qHBsAg levels and performed correlation analyses. Linear regression analysis revealed a correlation between CD39 expression, mitochondrial polarisation and quantitative HBsAg (qHBsAg) levels for HBV polymerase$_{455\text{-}463}$-specific responses, while no such correlation was found for HBV core$_{18\text{-}27}$-specific CD8$^+$ T cell responses (figure 5E,F). This suggests that antigen recognition drives the metabolic and exhaustion programme in polymerase$_{455\text{-}463}$-specific CD8$^+$ T cell responses but that this differs in HBV core$_{18\text{-}27}$-specific CD8$^+$ T cell responses.

Increased transaminase levels correlate with mitochondrial depolarisation in PD-1$^+$CD127$^-$ virus-specific CD8$^+$ T cells in chronic HCV infection

The differentiation of exhausted T cells is strongly influenced by viral antigen but is also subject to inflammatory cues. In DAA therapy during HCV infection, we had observed a negative correlation of mitochondrial polarisation with ALT (figure 4D), however, the control of viral replication and

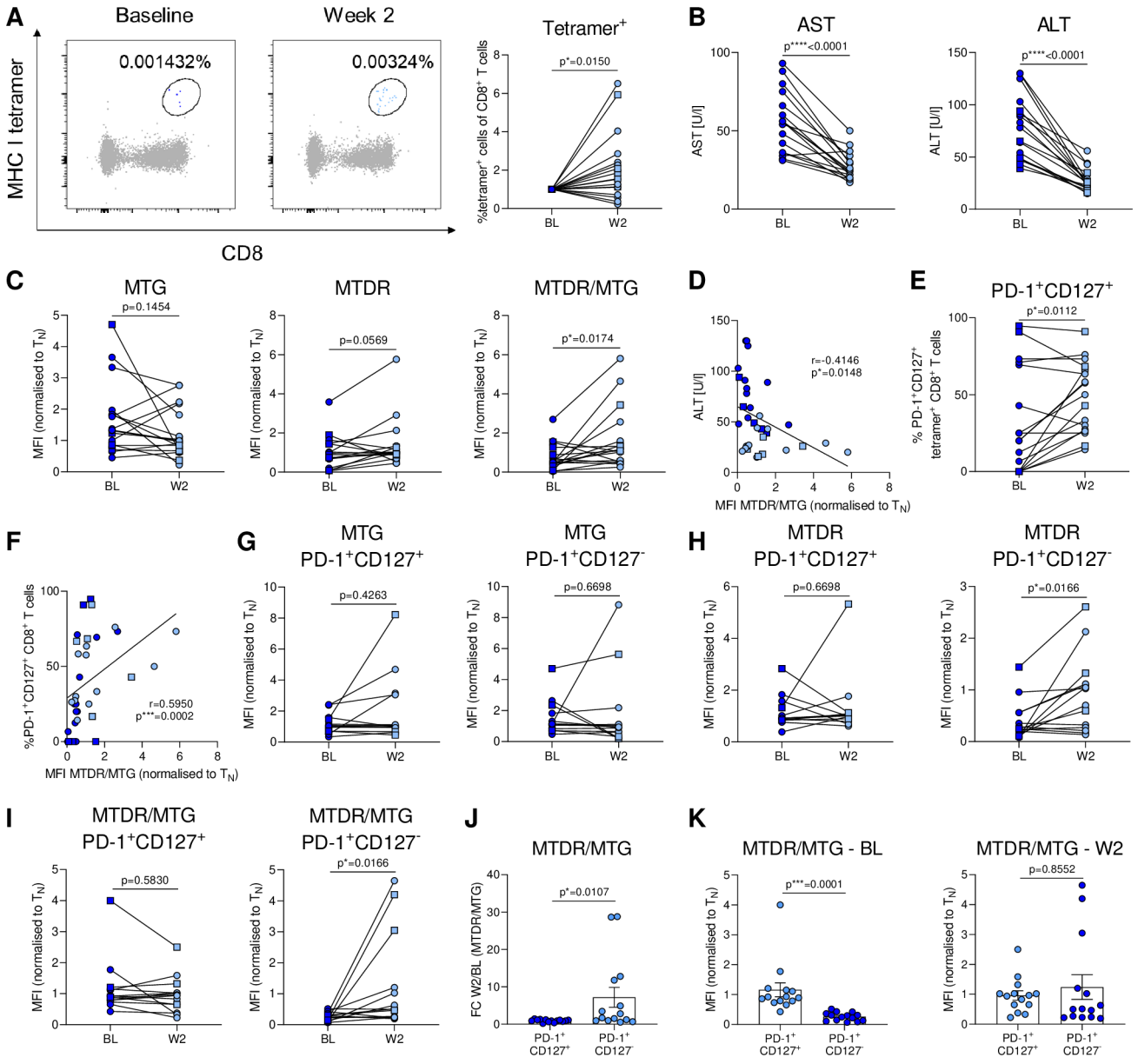

Figure 4 DAA therapy improves mitochondrial fitness of HCV-specific CD8$^+$ T cells. cHCV patients were analysed before and during DAA therapy. (A) Tetramer analysis of HCV-specific CD8$^+$ T cells at baseline (BL) and after 2 weeks of therapy (W2). (B) Serum transaminase levels at baseline and week 2. (C) Metabolic *ex vivo* staining of HCV-specific CD8$^+$ T cells for mitochondrial mass (MTG), mitochondrial membrane potential (MTDR) and mitochondrial polarisation (MTDR/MTG) at BL and W2 time points. (D) Correlation analysis of ALT concentration and mitochondrial polarisation at BL and W2. (E) Frequency of PD-1$^+$CD127$^+$ HCV-specific CD8$^+$ T cells at BL and W2. (F) Correlation of PD-1$^+$CD127$^+$ HCV-specific CD8$^+$ T cells with mitochondrial function. *Ex vivo* FACS analysis of (G) MTG, (H) MTDR and (I) mitochondrial polarisation (MTDR/MTG) of PD-1$^+$CD127$^+$ or PD-1$^+$CD127$^-$ HCV-specific CD8$^+$ T cells during DAA therapy. (J) Fold change of mitochondrial polarisation between W2 and BL was compared between PD-1$^+$CD127$^+$ and PD-1$^+$CD127$^-$ subsets. (K) Mitochondrial polarisation of PD-1$^+$CD127$^+$ and PD-1$^+$CD127$^-$ subsets at BL and W2 was compared. Metabolic staining intensity was normalised to naïve CD8$^+$ T cells from the same sample. HCV NS3$_{1073\text{-}1081}$ epitopes and HCV NS3$_{1406\text{-}1415}$ epitopes are represented by blue circles and squares, respectively. Wilcoxon test was performed in (A–C) and (G–K). Paired t-test was performed in (E). Spearman r correlation analyses were performed in (D, F). P values are indicated (p*<0.05, p***<0.005, p****<0.001). Error bars indicate mean±SEM. DAA, direct-acting antiviral; HCV, hepatitis C virus.

resolution of liver inflammation are intertwined. Therefore, we next investigated the connection of the metabolic T cell phenotype with the clinical activity in chronic HBV and HCV infection. Patients with cHCV infection displayed a diverse range of liver inflammation as indicated by aspartate aminotransferase (AST) and alanine aminotransferase (ALT) enzyme activity and viral loads, while in our cohort, HBV patients had milder hepatic inflammation (online supplemental figure 2A,B, online supplemental tables 1 and 2). We observed an inverse relationship of liver transaminases and mitochondrial polarisation and activation/exhaustion state of HCV-specific CD8$^+$ T cells but not in HBV infection (online supplemental figure 2C–L). There was no clear correlation with viral load as measured by PCR, however, it is unclear if that readout is a good measure of T cell antigen recognition (online supplemental figure

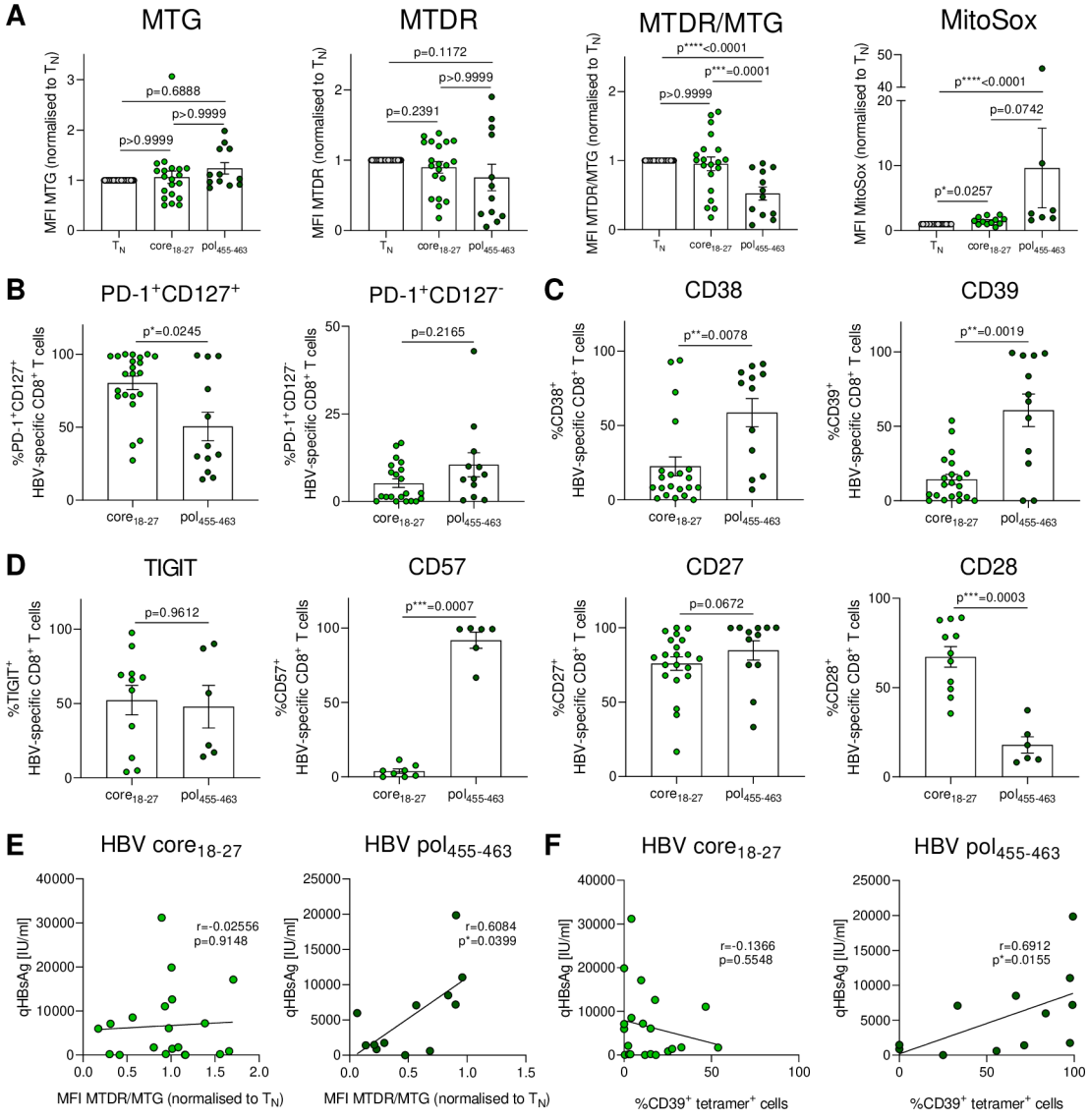

Figure 5 HBV $core_{18-27}$- and $polymerase_{455-463}$-specific $CD8^+$ T cells exhibit distinct metabolic and exhaustion features and are differentially associated with viral load. (A) HBV-specific $CD8^+$ T cells isolated from therapy-naïve cHBV patients were analysed *ex vivo* for mitochondrial mass (MTG), mitochondrial mass and membrane potential (MTDR), mitochondrial polarisation (MTDR/MTG), mitochondrial ROS (MitoSox) and (B) frequencies of PD-1^+CD127^+, PD-1^+CD127^-, (C) $CD38^+$, $CD39^+$, (D) $TIGIT^+$, $CD57^+$, $CD27^+$ and $CD28^+$ cells. (E) Correlation analyses of quantitative HBs antigen (qHBsAg) and mitochondrial polarisation and (F) frequencies of $CD39^+$ $tetramer^+$ cells are shown for HBV $core_{18-27}$- and $polymerase_{455-463}$-specific $CD8^+$ T cells. Metabolic staining intensity was normalised to naïve $CD8^+$ T cells from the same sample. HBV $core_{18-27}$- and $polymerase_{455-463}$-specific $CD8^+$ T cells are visualised by light green and dark green circles, respectively. Kruskal-Wallis test was performed in (A). Mann-Whitney U test was performed in (B–D). Spearman r correlation analyses were perfomed in (E, F). P values are indicated (p*<0.05, p**<0.01, p***<0.005, p****<0.001). Error bars indicate mean±SEM. HBV, hepatitis B virus.

3A–D). There was no direct correlation of metabolic T cell features and transaminase levels in HBeAg-negative chronic infection (ENCI) and HBeAg-negative chronic hepatitis B (ENCHB) patients (online supplemental figure 3E–H). These data show a link between the mitochondrial impairment of more severely exhausted virus-specific $CD8^+$ T cells and the degree of hepatic inflammation in cHCV infection.

Enolase expression is reduced in severely exhausted $CD8^+$ T cells and correlates with mitochondrial membrane potential

Our data demonstrate a prominent role for mitochondrial depolarisation in severely exhausted $CD8^+$ T cells. However, this depolarisation occurred despite high glucose uptake by HCV-specific $CD8^+$ T cells (figure 2D) and despite reduced utilisation of glucose for glycolysis in the metabolic flux analysis (online supplemental figure 1). We, therefore, sought to understand whether glycolytic flux was altered due to dysregulation of enzymes required for glycolysis (figure 6A). MRNA analysis identified variable expression of glycolytic genes between HBV-specific, HCV-specific and CMV-specific $CD8^+$ T cells (online supplemental figure 4A). We focused on the analysis of *Eno1* (encoding enolase 1) (online supplemental figure 4B). Intracellular staining for ENO1 revealed highest expression in naïve $CD8^+$ T cells, and reduced expression in HCV $NS3_{1073-1081}$-specific and $NS3_{1406-1415}$-specific $CD8^+$ T cells compared with HBV $core_{18-27}$-specific and $polymerase_{455-463}$-specific $CD8^+$ T cells (figure 6B).

We next investigated the relationship between exhausted T cell subsets and ENO1 expression. ENO1 was significantly more highly expressed in the metabolically fit PD-1$^+$CD127$^+$ subset compared to PD-1$^+$CD127$^-$ virus-specific CD8$^+$ T cells in chronic HBV and HCV infection (figure 6C). ENO1 expression was inversely correlated with the expression of activation/exhaustion marker CD38, but not with CD39 (figure 6D, online supplemental figure 4C). However, ENO1 expression positively correlated with mitochondrial polarisation (figure 6E), and there was a trend towards decreased mitochondrial ROS with increasing ENO1 expression (online supplemental figure 4D) in line with a model in which enolase levels more directly impact mitochondrial polarisation and low levels of enolase downstream predispose the cell to mitochondrial ROS production. Interestingly, elevated ALT levels also inversely correlated with ENO1, whereas AST levels, viral loads and qHBsAg did not (figure 6F, online supplemental figure 4E-G). These data indicated that ENO1 was expressed by T cells with less severe exhaustion and better mitochondrial fitness, and provoked the hypothesis that ENO1 could support the mitochondrial function of virus-specific CD8$^+$ T cells, counteracting exhaustion.

Enolase enzymatic activity controls virus-specific CD8$^+$ T cell metabolism by regulating glycolytic flux

To investigate the functional role of ENO1, we performed extracellular flux analysis of expanded HBV-specific and HCV-specific CD8$^+$ T cells and analysed their glycolytic capacity in the presence of enolase inhibitor[23] (online supplemental figure 5A–G) and/or after addition of the downstream metabolite pyruvate. Metabolic flux analysis showed that enolase inhibition reduced glycolysis in HBV-specific and HCV-specific CD8$^+$ T cells (online supplemental figure 5B,E). However, the drop in glycolysis could be overcome by simultaneous injection of the downstream metabolite pyruvate (online supplemental figure 5B,E). Interestingly, enolase inhibition did not cause changes in oxygen consumption, but pyruvate addition caused an immediate small drop in OCR, suggesting that the effects on glycolysis were dominant (online supplemental figure 5C,F). Comparison of the effect of enolase inhibition on glycolysis showed that HBV-specific CD8$^+$ T cells were enriched in strong responders to enolase inhibition compared with HCV-specific CD8$^+$ T cells, suggesting a stronger role of enolase for the glycolytic flux in these cells. This notion is in line with the higher expression levels of enolase observed in HBV-specific CD8$^+$ T cells (figure 6B). The dominant effect of enolase inhibition on glycolysis was also observed when cells were exposed to inhibitor pretreatment before the extracellular flux analysis (online supplemental figure 5H–I). Thus, enolase can act as a glycolytic checkpoint in HBV-specific and HCV-specific CD8$^+$ T cells and pyruvate can bypass enolase inhibition for enhanced glycolysis.

Enolase 1 inhibition can drive mitochondrial depolarisation in primary human CD8$^+$ T cells

Since short-term effects of enolase inhibition on respiration in *in vitro* metabolic flux assays were limited, but the correlations of enolase and mitochondrial respiration were strong in *ex vivo* analysis, we next asked if prolonged regulation of glycolysis via ENO1 would also impact on mitochondrial polarisation of freshly isolated primary human CD8$^+$ T cells and treated CD8$^+$ T cells from healthy individuals overnight with an enolase-specific inhibitor. We observed that ENO1 inhibition resulted in significantly reduced mitochondrial polarisation, more depolarised mitochondria and trends towards reduced cytokine production (online supplemental figure 4H,I). Thus, ENO1 inhibition resulted in a mitochondrial phenotype typical for severely exhausted virus-specific CD8$^+$ T cells.

Enolase enzymatic activity controls virus-specific CD8$^+$ T cell effector function

Due to the prominent role of glycolysis for T cell effector function, we next wondered if enolase would represent a metabolic regulator of exhausted T cell function in virus-specific CD8$^+$ T cells. We, therefore, examined cytokine production of HBV core$_{18\text{-}27}$-specific and HCV NS3$_{1073\text{-}1081}$-specific, NS3$_{1406\text{-}1415}$-specific and NS5B$_{2594\text{-}2602}$-specific CD8$^+$ T cells after overnight treatment with AP-III-a4 hydrochloride or in combination with pyruvate. Treatment did not affect viability (online supplemental figure 4J). After treatment with the ENO1 inhibitor, HBV-specific and HCV-specific CD8$^+$ T cells showed a significant drop in IFN-γ production (figure 6G). In contrast, the addition of pyruvate enhanced cytokine production (figure 6H–L, online supplemental figure 4K-M). The effects of enolase inhibition on IFN-γ production were stronger than on TNF-α production, however, pyruvate supplementation also enhanced the production of this cytokine, in particular in HCV-specific CD8$^+$ T cells (figure 6J).

Enolase 1 expression is reduced in exhausted versus memory-like CD8$^+$ T cells in HBV infection in mice

To understand the role of differential ENO1 expression in hepatitis virus-specific CD8$^+$ T cell exhaustion in the same virus model and intrahepatic environment, and to understand differences between acute and chronic infection, we used a recently developed mouse model of acute or chronic HBV infection.[24] In this model, C57Bl/6 mice were infected with different doses of an adenoviral vector encoding for a 1.3-overlength HBV genome (Ad-HBV-Luc) after transfer of naïve HBV Cor$_{93}$-specific CD8$^+$ T cells. Depending on the dose of Ad-HBV-Luc administered, mice develop either acute self-limiting (10^7 pfu) or chronic HBV infection (10^8 pfu) (figure 7A). At 15 dpi and 30 dpi, respectively, liver-associated lymphocytes were isolated and Cor$_{93}$-specific CD8$^+$ T cells were analysed by single-cell RNA-seq. UMAP analysis identified different antigen-specific T cell transcriptomes in acute and chronic infection (figure 7B). Clustering analysis revealed four separate clusters with differential expression of exhaustion markers (figure 7C). HBV-specific CD8$^+$ T cells from mice with acute HBV infection were predominantly enriched in cluster 1 (C1). Chronic HBV-specific CD8$^+$ T cells were enriched in C4 (figure 7D). Markers associated with severe exhaustion, such as *Pdcd1*, *Cd38*, *Cd39*, *Tox* and *Fli1* showed increased expression in C4 (figure 7E). In contrast, C1 highly expressed *Il7r*, *Tcf7*, *Slamf6* and *Cxcr5* that indicate homeostatic and memory-like characteristics. Interestingly, *Eno1* expression was significantly higher in acute compared with chronic HBV-specific CD8$^+$ T cells, indicating a loss of enolase expression during chronic infection (figure 7F). GSEA of exhaustion signatures revealed a significant enrichment of exhaustion genes in HBV-specific CD8$^+$ T cells isolated from chronic condition, as expected. Moreover, direct comparison of C1 versus C4 showed a significant enrichment of exhaustion-associated gene expression in C4 and an enrichment of memory-associated features in C1 (figure 7G).[25 26] Moreover, C1 was significantly enriched for *Eno1* expression compared with other clusters (figure 7H). These results are in line with our previous findings on ENO1 expression in less severely exhausted virus-specific CD8$^+$ T cells in cHBV and cHCV patients (figure 6C). Moreover, we observed significantly elevated glycolytic gene expression in acute versus chronic cells, with C1

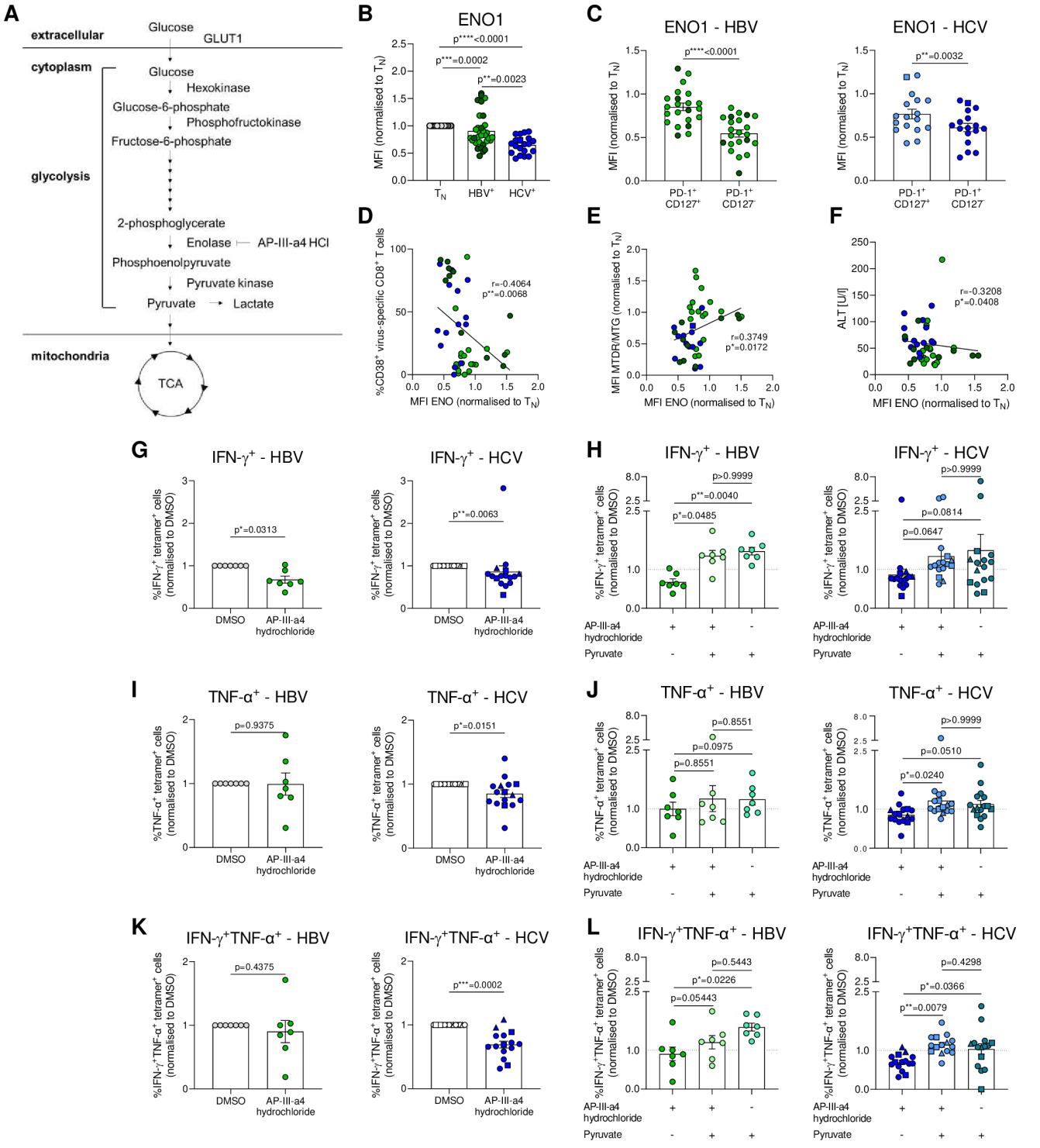

Figure 6 ENO1 lowly expressed in severely exhausted virus-specific CD8$^+$ T cells is a metabolic checkpoint controlling glycolytic flux and T cell function. (A) Schematic overview of the glycolytic pathway. (B) Intracellular ENO1 staining of HBV-specific and HCV-specific CD8$^+$ T cells. ENO1 MFIs are normalised to naïve CD8$^+$ T cells of the respective donor. (C) *Ex vivo* analysis of PD-1$^+$CD127$^+$ and PD-1$^+$CD127$^-$ subsets of HBV-specific and HCV-specific CD8$^+$ T cells for ENO1 expression. (D) Correlation analyses of ENO1 expression and frequencies of CD38$^+$ virus-specific CD8$^+$ T cells. (E) Correlation analyses of ENO1 expression and mitochondrial polarisation (MTDR/MTG) of HBV-specific and HCV-specific CD8$^+$ T cells. (F) Correlation analysis of ENO1 expression and serum ALT level of therapy-naïve cHBV and cHCV patients. (G–L) IFN-γ and TNF-α production of PMA-stimulated and ionomycin-stimulated hepatitis virus-specific CD8$^+$ T cells after o/n treatment with DMSO, AP-III-a4 hydrochloride (10 µM) and/or sodium pyruvate (2 mM). Cytokine secretion is shown normalised to DMSO-treated hepatitis virus-specific CD8$^+$ T cells as control samples. HBV core$_{18\text{-}27}$- and polymerase$_{455\text{-}463}$-specific CD8$^+$ T cells are visualised by light green and dark green circles, respectively. HCV NS3$_{1073\text{-}1081}$, HCV NS3$_{1406\text{-}1415}$ and HCV NS5B$_{2594\text{-}2602}$ epitopes are represented by blue circles, squares and triangles, respectively. Kruskall-Wallis test was performed in (B). Paired t-test was performed in (C). Spearman r correlation analyses were performed in (D–F). Wilcoxon test was performed in (G), (I, K). Friedman test was performed in (H), (J) and (L, left). Two-way ANOVA was performed in (L, right). P values are indicated (p*<0.05, p**<0.01, p***<0.005, p****<0.001). Error bars indicate mean±SEM. ANOVA, analysis of variance; cHBV, chronic hepatitis B virus; HCV, hepatitis C virus.

exhibiting highest expression of glycolytic genes among all clusters, as well as an enrichment of genes responsible for OXPHOS in acute versus chronic HBV infection. In sum, these data support a role for enolase in metabolically regulating differential exhaustion profiles of intrahepatic virus-specific CD8$^+$ T cells (figure 7I).

DISCUSSION

T cell exhaustion is a prominent feature of virus-specific CD8$^+$ T cells in chronic HBV and HCV infection and linked to metabolic changes. Here, by performing a detailed comparison of the metabolic states of HBV core$_{18\text{-}17}$-specific and polymerase$_{455\text{-}463}$-specific and HCV NS3$_{1073\text{-}1081}$-specific, NS3$_{1406\text{-}1415}$-specific and NS5B$_{2594\text{-}2602}$-specific CD8$^+$ T cells from patients with chronic infection, we identified major differences in the metabolism of virus-specific CD8$^+$ T cell responses with pronounced mitochondrial dysregulation in severely exhausted PD-1$^+$CD127$^-$ CD8$^+$ T cells enriched in chronic HCV infection. In contrast, higher mitochondrial fitness was observed in PD1$^+$CD127$^+$ CD8$^+$ T cells that have also been termed 'memory-like' due to their homeostatic features.[7 25] Interestingly, the link between metabolism and exhaustion subtype was independent of the viral aetiology. In cHCV infection, the metabolic state also correlated with the extent of liver inflammation. In cHBV infection, we observed different roles for different HBV-specific CD8$^+$ T cell responses. In particular, HBV polymerase$_{455\text{-}463}$-specific CD8$^+$ T cells showed a more severe mitochondrial dysfunction that correlated with viral antigen levels, while HBV core$_{18\text{-}27}$-specific CD8$^+$ T cell responses were enriched in the PD1$^+$CD127$^+$ exhaustion phenotype, had relatively intact metabolism but also did not show a clinical correlation. Taken together, these findings suggested a conserved mechanism of metabolic programming in exhausted T cells across viral aetiologies and suggested specific metabolic checkpoints governing different exhaustion states. We identified differential enolase expression as a potential metabolic regulator and speculated if it controls the exhaustion states. Indeed, enolase inhibition resulted in reduced metabolic flux and mitochondrial depolarisation. Bypassing enolase regulation in HBV-specific and HCV-specific CD8$^+$ T cells augmented their glycolysis and T cell effector function. In sum, these findings indicate that hepatitis virus-specific CD8$^+$ T cells in cHBV and cHCV infection have different exhaustion states due to distinct metabolic programmes. The identification of enolase 1 as a contributing regulator of these exhaustion programmes may provide opportunities for targeted intervention.

Persistent antigen stimulation is a major driver of T cell exhaustion.[27] DAA therapy in chronic HCV infection causes rapid inhibition of viral replication and served as an *in vivo* model to analyse the effect of tuning viral antigen and associated liver inflammation. Our analysis showed that after 2 weeks of DAA therapy, HCV-specific CD8$^+$ T cell metabolism improved with enhanced mitochondrial polarisation. The impact of DAA therapy on T cell metabolism has also been investigated by Aregay *et al*. who, however, did not find a major effect on mitochondrial HCV-specific CD8$^+$ T cell metabolism.[11] In contrast, our DAA therapy results fit to work by Barili *et al*. who also observed improved mitochondrial polarisation in HCV-specific CD8$^+$ T cells by focusing on epitope-matched virus-specific CD8$^+$ T cell responses.[22] In these studies, different types of exhaustion subsets were not analysed in detail. In our work, the enhanced mitochondrial fitness after DAA therapy was clearly linked to an accumulation of PD1$^+$CD127$^+$ virus-specific CD8$^+$ T cells. However, our data also suggest that more exhausted subsets experience stronger improvement in metabolism by DAA therapy. Thus, different distributions of exhausted T cell subsets at baseline time points may contribute to the different results found in these earlier studies.[11 22] Interestingly, while we observed a correlation of the metabolic state of HCV-specific CD8$^+$ T cells with liver inflammation that is intertwined with viral replication and antigen recognition, we did not observe such a correlation with liver inflammation in chronic HBV infection. However, in cHBV infection we observed clearly distinct roles for HBV core$_{18\text{-}27}$-specific and polymerase$_{455\text{-}463}$-specific responses, in line with previous results from phenotypic and functional profiling.[9] HBV polymerase$_{455\text{-}463}$-specific CD8$^+$ T cell responses displayed more diverse metabolic and exhaustion states. Importantly, we also observed correlations of activation and mitochondrial dysfunction in HBV polymerase$_{455\text{-}463}$-specific CD8$^+$ T cell responses with qHBsAg levels in these patients, suggesting that the exhaustion state and the associated metabolism of HBV polymerase$_{455\text{-}463}$-specific CD8$^+$ T cell response is due to the degree of antigen recognition in cHBV infection. These findings also suggest that antigen is a dominant driver of exhausted T cell metabolism in our cohort, although a contribution of the inflammatory microenvironment, in particular in cHCV infection, cannot be formally excluded.

Glycolysis is key to effector T cell differentiation and function and subject to regulation by immune checkpoints.[14 17 18 28] Here, in established human chronic infection, we observed high glucose uptake but reduced metabolic activity in severely exhausted CD8$^+$ T cells. These cells showed significant mitochondrial disturbances similar to exhausted T cells in LCMV or tumour models.[18 29–31] It was puzzling that these exhausted T cells also had high glucose uptake despite limited glycolysis and mitochondrial impairment, which prompted us to dissect the glycolytic pathway. Our analysis revealed reduced ENO1 expression in severely exhausted PD-1$^+$CD127$^-$ CD8$^+$ T cells enriched in chronic HCV infection. Inhibition of ENO1 resulted in decreased glycolytic function that could be reversed by downstream pyruvate supplementation. These results are consistent with work that identified reduced enolase activity associated with insufficient effector function in tumour-infiltrating lymphocytes which was reversed after checkpoint therapy.[23] It also fits to the notion that enolase can act as a metabolic checkpoint, as illustrated by its role in governing the differentiation of regulatory T cells.[32] Enolase is upstream of the production of PEP, a glycolytic intermediate important for sustaining T cell receptor-mediated Ca^{2+}-NFAT signalling and effector functions by repressing sarco/ER Ca^{2+}-ATPase (SERCA) activity.[17] Reduced enolase activity may therefore limit calcium signalling which may in turn explain the reduced T cell function observed after enolase inhibition. Some HCV-specific CD8$^+$ T cell responses with low glycolytic activity were metabolically unresponsive to enolase inhibition, suggesting a lack of enolase enzymatic activity in those cells. However, this was a rather extreme observation in our cohort, since most exhausted CD8$^+$ T cell responses analysed had residual enolase activity. We also observed reduced mitochondrial polarisation and OXPHOS after overnight ENO1 inhibition, suggesting that enolase provides metabolic substrates for the TCA cycle and its regulation could be involved in throttling metabolic flux upstream of the mitochondrial changes in exhausted T cells. In sum, enolase serves as a metabolic checkpoint of exhausted CD8$^+$ T cells in viral hepatitis.

Our data demonstrate that HBV-specific and HCV-specific CD8$^+$ T cells exhibit distinct metabolic profiles during chronic infection associated with differences in their exhaustion programmes that are linked to antigen recognition and in cHCV infection, with liver inflammation. We identified the glycolytic enzyme enolase as an upstream metabolic checkpoint contributing to the regulation of the metabolic and functional

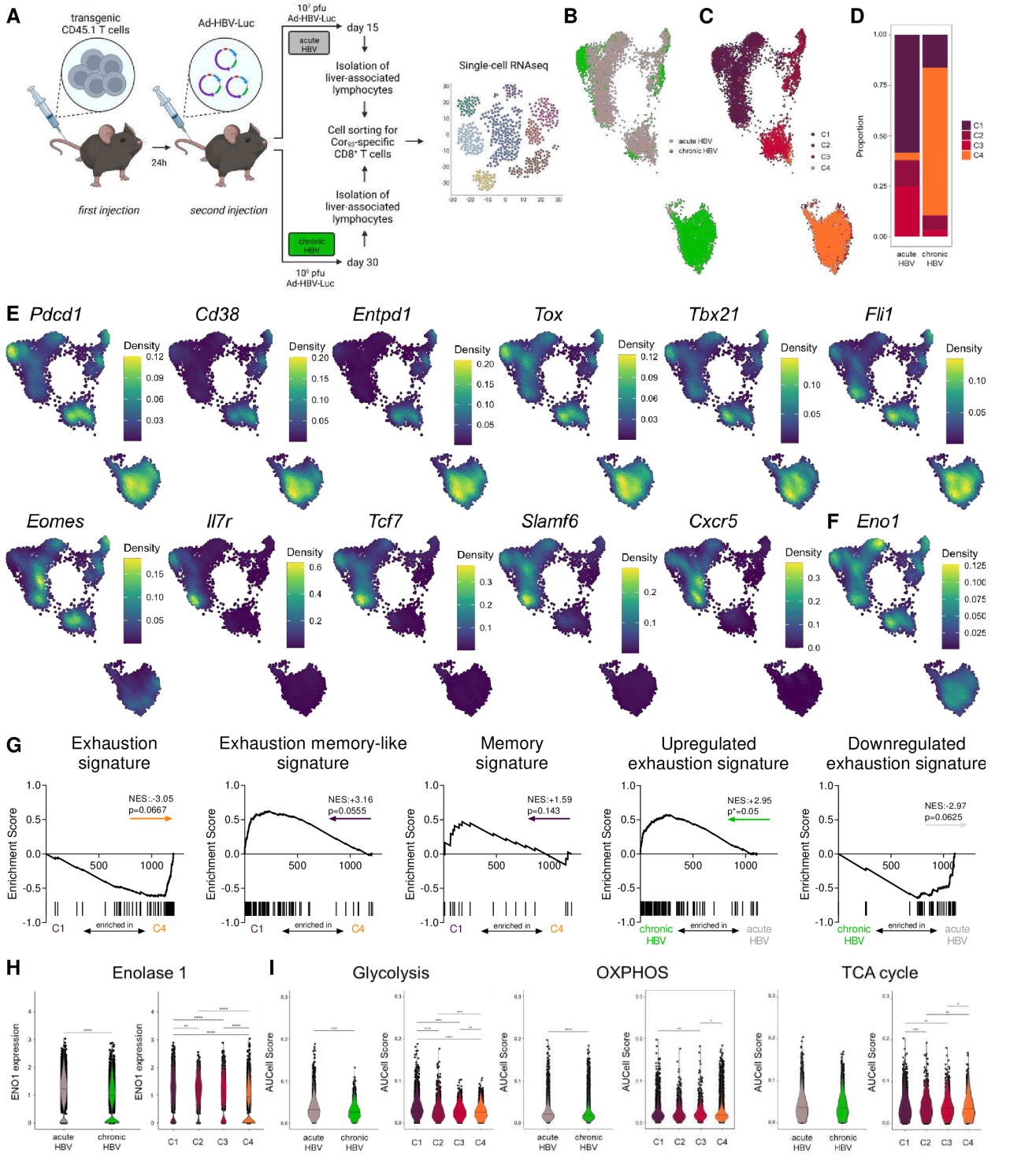

Figure 7 Differential enolase 1 expression is linked to different metabolic programmes and exhaustion severities in acute versus chronic HBV infection. (A) Schematic illustration depicting experimental procedure. C57Bl/6 mice were intravenously injected with 10 000 transgenic CD45.1 T cells derived from Cor_{93} TCR-transgenic mice and after 24 hours infected with 10^7 (acute self-limiting) or 10^8 pfu (chronic) of adenoviral vector (Ad-HBV-Luc). Liver-associated lymphocytes were isolated after 15 (acute) or 30 days (chronic) and subsequently sorted for Cor_{93}-specific $CD8^+$ T cells. Single-cell RNA sequencing was performed on 3000 Cor_{93}-specific cells per mouse. (B) UMAP projection showing Cor_{93}-specific $CD8^+$ T cells coloured by condition (C) and cluster identity. (D) Ratio of the number of cells in each cluster in acute and chronic samples. (E) Densities of gene expression levels are visualised by Nebulosa for selected genes and (F) Eno1. (G) GSEA plots comparing the differentially expressed genes (DEGs) for cluster 1 (C1) versus cluster 4 (C4) with the signatures reported in Utzschneider *et al.*[25] (Exhaustion, Exhaustion memory-like and Memory signatures) and the DEGs of acute versus chronic conditions compared with the signatures published in Bengsch *et al.*[26] (Upregulated and downregulated epigenomic exhaustion signatures). Coloured arrows indicate the cluster or condition in which the gene set is enriched. (H) Enolase 1 expression in acute versus chronic setting and cluster 1–4 across conditions. (I) Pathway scores of glycolysis, TCA cycle and oxidative phosphorylation of acute versus chronic setting and among clusters. Mann-Whitney test was performed in (H–I). P values are indicated (p*<0.05, p**<0.01, p***<0.005, p****<0.001). HBV, hepatitis C virus.

programmes. Boosting enolase function could represent a novel strategy to counteract reduced effector function of virus-specific CD8$^+$ T cells in chronic viral hepatitis.

Author affiliations
[1]Clinic for Internal Medicine II, Freiburg University Medical Center, Faculty of Medicine, University of Freiburg, Freiburg im Breisgau, Germany
[2]Faculty of Biology, University of Freiburg, Freiburg im Breisgau, Germany
[3]Health Data Science Unit, Medical Faculty, University of Heidelberg, Heidelberg, Germany
[4]Max Planck Institute of Immunobiology and Epigenetics, Freiburg im Breisgau, Germany
[5]Institute of Neuropathology, Freiburg University Medical Center, Faculty of Medicine, University of Freiburg, Freiburg im Breisgau, Germany
[6]Signalling Research Centres BIOSS and CIBSS, University of Freiburg, Freiburg im Breisgau, Germany
[7]Translational Biomarkers, Infectious Diseases Therapeuic Area, Janssen Pharmaceutica, Beerse, Belgium
[8]Division of Infection and Immunity, Cardiff University School of Medicine, Cardiff University, Cardiff, UK
[9]Systems Immunity Research Institute, Cardiff University School of Medicine, Cardiff, UK
[10]Institute of Virology, Freiburg University Medical Center, Faculty of Medicine, University Hospital Freiburg, Freiburg im Breisgau, Germany
[11]The Bloomberg-Kimmel Institute for Cancer Immunotherapy, Johns Hopkins Medicine Sidney Kimmel Comprehensive Cancer Center, Baltimore, Maryland, USA
[12]Institute for Medical Microbiology, Immunology and Hygiene, Technical University of Munich (TUM), Munich, Germany
[13]Department of General Pediatrics, Laboratory of Clinical Biochemistry and Metabolism, Medical Center-University of Freiburg, Adolescent Medicine and Neonatology, Faculty of Medicine, University of Freiburg, Freiburg, Germany
[14]German Center for Infection Research (DZIF), Munich Partner Site, Munich, Germany
[15]Institute of Molecular Immunology, Klinikum Rechts der Isar, Technical University of Munich, Munich, Germany
[16]German Cancer Consortium (DKTK), Partner Site Freiburg, Heidelberg, Germany

Acknowledgements We would like to thank all participants who contributed to this study. We thank J. Wersing and the Lighthouse Core Facility for help with cell sorting. The graphical abstract was created using BioRender.com.

Contributors FW performed the experiments and analysed the data with the help of AVH, CR, EN, OGorka, LH and NR. BM performed sorting of hepatitis virus-specific CD8$^+$ T cells and analysed transcriptomic data with the help of JA and SEJ. SL-L and DAP provided the peptide-MHC class I monomers. MP collected clinical data. FW and BB wrote the manuscript. MV, ELP, OGroß, CMH, PK, DW, KS, CN-H, TB, RT and MH proofread the manuscript and revised it for important intellectual content. BB designed and supervised the study, accepts full responsibility for the work and the conduct of the study, had access to the data and controlled the decision to publish.

Funding This study was supported by grants from the Deutsche Forschungsgemeinschaft (DFG, German Research Foundation, TRR179 project no. 272983813, project no. 520992132, SFB1160 project no. 256073931, SFB1479 project no. 441891347 and CIBSS-EXC-2189 project no. 390939984). DAP was supported by a Wellcome Trust Senior Investigator Award (100326/Z/12/Z).

Competing interests None declared.

Patient and public involvement Patients and/or the public were not involved in the design, or conduct, or reporting, or dissemination plans of this research.

Patient consent for publication Consent obtained directly from patient(s).

Ethics approval This study involves samples from human participants recruited through the HBUF/FREEZE biobank and was approved by the Ethics Committee of the Albert-Ludwigs University, Freiburg 243/18, 474/14. Participants gave informed consent to participate in the study prior to enrolment.

Provenance and peer review Not commissioned; externally peer reviewed.

Data availability statement Data are available on reasonable request.

ORCID iDs
David A Price http://orcid.org/0000-0001-9416-2737
Tobias Boettler http://orcid.org/0000-0002-1195-055X
Maike Hofmann http://orcid.org/0000-0001-8410-8833
Robert Thimme http://orcid.org/0000-0003-1417-4135
Bertram Bengsch http://orcid.org/0000-0003-2552-740X

REFERENCES

1 Boni C, Fisicaro P, Valdatta C, *et al*. Characterization of hepatitis B virus (HBV)-specific T-cell dysfunction in chronic HBV infection. *J Virol* 2007;81:4215–25.
2 Bengsch B, Seigel B, Ruhl M, *et al*. Coexpression of PD-1, 2B4, CD160 and KLRG1 on exhausted HCV-specific CD8+ T cells is linked to antigen recognition and T cell differentiation. *PLOS Pathog* 2010;6:e1000947.
3 Acerbi G, Montali I, Ferrigno GD, *et al*. Functional reconstitution of HBV-specific CD8 T cells by in vitro polyphenol treatment in chronic hepatitis B. *J Hepatol* 2021;74:783–93.
4 Maini MK, Boni C, Lee CK, *et al*. The role of virus-specific CD8(+) cells in liver damage and viral control during persistent hepatitis B virus infection. *J Exp Med* 2000;191:1269–80.
5 Wolski D, Foote PK, Chen DY, *et al*. Early transcriptional divergence marks virus-specific primary human CD8$^+$ T cells in chronic versus acute infection. *Immunity* 2017;47:648–63.
6 Bengsch B, Martin B, Thimme R. Restoration of HBV-specific CD8+ T cell function by PD-1 blockade in inactive carrier patients is linked to T cell differentiation. *J Hepatol* 2014;61:1212–9.
7 Wieland D, Kemming J, Schuch A, *et al*. Tcf1(+) hepatitis C virus-specific CD8(+) T cells are maintained after cessation of chronic antigen stimulation. *Nat Commun* 2017;8:15050.
8 Utzschneider DT, Legat A, Fuertes Marraco SA, *et al*. T cells maintain an exhausted phenotype after antigen withdrawal and population Reexpansion. *Nat Immunol* 2013;14:603–10.
9 Schuch A, Salimi Alizei E, Heim K, *et al*. Phenotypic and functional differences of HBV core-specific versus HBV polymerase-specific CD8+ T cells in chronically HBV-infected patients with low viral load. *Gut* 2019;68:905–15.
10 Hensel N, Gu Z, Sagar S, *et al*. Memory-like HCV-specific CD8(+) T cells retain a molecular scar after cure of chronic HCV infection. *Nat Immunol* 2021;22:229–39.
11 Aregay A, Owusu Sekyere S, Deterding K, *et al*. Elimination of hepatitis C virus has limited impact on the functional and mitochondrial impairment of HCV-specific CD8+ T cell responses. *J Hepatol* 2019;71:889–99.
12 Abdel-Hakeem MS, Manne S, Beltra J-C, *et al*. Author correction: epigenetic scarring of exhausted T cells hinders memory differentiation upon eliminating chronic Antigenic stimulation. *Nat Immunol* 2021;22:1465.
13 Yates KB, Tonnerre P, Martin GE, *et al*. Epigenetic scars of CD8(+) T cell exhaustion persist after cure of chronic infection in humans. *Nat Immunol* 2021;22:1020–9.
14 Chang C-H, Curtis JD, Maggi LB, *et al*. Posttranscriptional control of T cell Effector function by aerobic glycolysis. *Cell* 2013;153:1239–51.
15 Gubser PM, Bantug GR, Razik L, *et al*. Rapid Effector function of memory CD8+ T cells requires an immediate-early glycolytic switch. *Nat Immunol* 2013;14:1064–72.
16 Menk AV, Scharping NE, Moreci RS, *et al*. Early TCR signaling induces rapid aerobic glycolysis enabling distinct acute T cell Effector functions. *Cell Rep* 2018;22:1509–21.
17 Ho P-C, Bihuniak JD, Macintyre AN, *et al*. Phosphoenolpyruvate is a metabolic checkpoint of anti-tumor T cell responses. *Cell* 2015;162:1217–28.
18 Bengsch B, Johnson AL, Kurachi M, *et al*. Bioenergetic Insufficiencies due to metabolic alterations regulated by the inhibitory receptor PD-1 are an early driver of CD8(+) T cell exhaustion. *Immunity* 2016;45:358–73.
19 Scharping NE, Rivadeneira DB, Menk AV, *et al*. Mitochondrial stress induced by continuous stimulation under hypoxia rapidly drives T cell exhaustion. *Nat Immunol* 2021;22:205–15.
20 Schurich A, Pallett LJ, Jajbhay D, *et al*. Distinct metabolic requirements of exhausted and functional virus-specific CD8 T cells in the same host. *Cell Rep* 2016;16:1243–52.
21 Fisicaro P, Barili V, Montanini B, *et al*. Targeting mitochondrial dysfunction can restore antiviral activity of exhausted HBV-specific CD8 T cells in chronic hepatitis B. *Nat Med* 2017;23:327–36.
22 Barili V, Fisicaro P, Montanini B, *et al*. Targeting P53 and Histone methyltransferases restores exhausted CD8+ T cells in HCV infection. *Nat Commun* 2020;11:604.
23 Gemta LF, Siska PJ, Nelson ME, *et al*. Impaired Enolase 1 glycolytic activity restrains effector functions of tumor-infiltrating CD8(+) T cells. *Sci Immunol* 2019;4:eaap9520.
24 Manske K, Schneider A, Ko C, *et al*. In vivo bioluminescence imaging of HBV replicating hepatocytes allows for the monitoring of anti-viral immunity. *Viruses* 2021;13:2273.
25 Utzschneider DT, Charmoy M, Chennupati V, *et al*. T cell factor 1-expressing memory-like CD8(+) T cells sustain the immune response to chronic viral infections. *Immunity* 2016;45:415–27.

26 Bengsch B, Ohtani T, Khan O, *et al*. Epigenomic-guided mass cytometry profiling reveals disease-specific features of exhausted CD8 T cells. *Immunity* 2018;48:1029–45.
27 Bucks CM, Norton JA, Boesteanu AC, *et al*. Chronic antigen stimulation alone is sufficient to drive CD8+ T cell exhaustion. *J Immunol* 2009;182:6697–708.
28 Chang C-H, Qiu J, O'Sullivan D, *et al*. Metabolic competition in the tumor microenvironment is a driver of cancer progression. *Cell* 2015;162:1229–41.
29 Yu Y-R, Imrichova H, Wang H, *et al*. Disturbed mitochondrial Dynamics in CD8(+) Tils reinforce T cell exhaustion. *Nat Immunol* 2020;21:1540–51.
30 Vardhana SA, Hwee MA, Berisa M, *et al*. Impaired mitochondrial oxidative phosphorylation limits the self-renewal of T cells exposed to persistent antigen. *Nat Immunol* 2020;21:1022–33.
31 Liu Y-N, Yang J-F, Huang D-J, *et al*. Hypoxia induces mitochondrial defect that promotes T cell exhaustion in tumor microenvironment through MYC-regulated pathways. *Front Immunol* 2020;11:1906.
32 De Rosa V, Galgani M, Porcellini A, *et al*. Glycolysis controls the induction of human regulatory T cells by modulating the expression of FOXP3 exon 2 splicing variants. *Nat Immunol* 2015;16:1174–84.

Supplemental tables

Supplemental table 1: cHBV cohort

Patient ID	Sex	Age (years)	Viral load (IU/ml)	AST (U/l)	ALT (U/l)	HBeAg	HBsAg (IU/ml)	Therapy	Genotype	HLA	Tetramer *ex vivo*
cHBV#1	male	65	<10	26	30	negative	nd	naïve	nd	A*02:01	$core_{18-27}$
cHBV#2	female	59	<10	28	32	negative	42.37	naïve	nd	A*02:01	$core_{18-27}$
cHBV#3	male	34	1531	28	45	negative	19848.26	naïve	D	A*02:01	$core_{18-27}$, $pol_{455-463}$
cHBV#4	male	53	15	54	217	negative	0.37	naïve	nd	A*02:01	$core_{18-27}$
cHBV#5	female	36	1033	19	17	negative	227.3	naïve	nd	A*02:01	$core_{18-27}$
cHBV#6	female	46	<10	16	8	negative	0.62	naïve	nd	A*02:01	$core_{18-27}$
cHBV#7	male	49	649	26	37	negative	nd	naïve	A	A*02:01	$core_{18-27}$, $pol_{455-463}$
cHBV#8	male	53	335	126	93	negative	183.92	naïve	D	A*02:01	$core_{18-27}$
cHBV#9	female	25	574	30	33	negative	nd	naïve	D	A*02:01	$core_{18-27}$, $pol_{455-463}$
cHBV#10	male	55	648	26	28	negative	nd	naïve	A	A*02:01	$core_{18-27}$
cHBV#11	male	32	nd	24	38	negative	nd	naïve	nd	A*02:01	$core_{18-27}$
cHBV#12	male	37	720	nd	37	negative	nd	naïve	D	A*02:01	$core_{18-27}$
cHBV#13	female	59	88	64	78	negative	200.97	naïve	A	A*02:01	$core_{18-27}$
cHBV#14	female	25	534	20	18	negative	1706.51	naïve	D	A*02:01	$core_{18-27}$
cHBV#15	male	24	<10	24	24	6.32	nd	naïve	nd	A*02:01	$pol_{455-463}$
cHBV#16	female	41	515	33	48	negative	7082.27	naïve	D	A*02:01	$core_{18-27}$, $pol_{455-463}$
cHBV#17	female	26	545	27	39	negative	17106.18	naïve	A	A*02:09	$core_{18-27}$
cHBV#18	male	50	25	52	102	nd	0.11	naïve	nd	A*02:01	$core_{18-27}$, $pol_{455-463}$
cHBV#19	male	30	3844	127	191	negative	11044.84	naïve	nd	A*02:02	$core_{18-27}$, $pol_{455-463}$
cHBV#20	male	55	196	37	29	nd	1661.31	naïve	nd	A*02:01	$core_{18-27}$
cHBV#21	male	38	5128	26	29	negative	851.61	naïve	nd	A*02:01	$core_{18-27}$, $pol_{455-463}$
cHBV#22	male	26	53584322	28	51	>120	1401.39	naïve	nd	A*02:01	$core_{18-27}$, $pol_{455-463}$
cHBV#23	female	35	52	77	36	negative	1739.63	naïve	nd	A*02:01	$core_{18-27}$, $pol_{455-463}$
cHBV#24	female	59	92090	48	72	negative	602.86	naïve	nd	A*02:01	$pol_{455-463}$
cHBV#25	female	32	955	26	21	nd	2127.53	naïve	nd	A*02:01	$core_{18-27}$
cHBV#26	female	39	101	23	21	negative	1460.9	naïve	D	A*02:01	$pol_{455-463}$
cHBV#27	male	54	883	22	29	negative	nd	naïve	nd	A*02:01	$core_{18-27}$
cHBV#28	female	21	1901	23	30	negative	12615.76	naïve	D	A*02:01	$core_{18-27}$
cHBV#29	female	40	1655	17	15	nd	555.63	naïve	nd	A*02:01	$core_{18-27}$
cHBV#30	female	36	3214	20	23	negative	6083.86	naïve	D	A*02:01	$core_{18-27}$
cHBV#31	female	28	425	19	18	negative	8508.7	naïve	nd	A*02:01	$core_{18-27}$, $pol_{455-463}$

Supplemental table 2: cHCV cohort

Patient ID	Sex	Age (years)	Viral load (IU/ml)	AST (U/l)	ALT (U/l)	Therapy*	Genotype	HLA	Tetramer *ex vivo*
cHCV#1	male	57	138330	70	102	Ledipasvir/Sofosbuvir	1a	A*02:01	$NS3_{1073-1081}$
cHCV#2	female	76	5301347	31	33	Ledipasvir/Sofosbuvir	1b	A*02:01	$NS3_{1073-1081}$
cHCV#3	male	45	5029509	31	52	Ledipasvir/Sofosbuvir	1a	A*02:01	$NS3_{1406-1415}$
cHCV#4	female	71	4370502	34	30	Ledipasvir/Sofosbuvir	5	A*02:01	$NS3_{1073-1081}$
cHCV#5	male	54	667940	121	100	Ledipasvir/Sofosbuvir/Ribavirin	1a	A*02:01	$NS3_{1073-1081}$
cHCV#6	male	45	2937310	51	89	Sofosbuvir/Daclatasvir	1a	A*02:01	$NS3_{1073-1081}$
cHCV#7	male	50	738876	130	182	Sofosbuvir/Velpatasvir	1a	A*02:01	$NS3_{1073-1081}$
cHCV#8	male	61	3287107	88	130	Ledipasvir/Sofosbuvir	1a	A*02:01	$NS3_{1073-1081}$
cHCV#9	male	50	293903	54	91	Ledipasvir/Sofosbuvir/Ribavirin	4	A*02:01	$NS3_{1073-1081}$
cHCV#10	female	75	9056623	56	54	Glecaprevir/Pibrentasvir	1b	A*02:01	$NS3_{1073-1081}$
cHCV#11	male	55	5822243	25	38	Ledipasvir/Sofosbuvir	1a	A*02:01	$NS3_{1073-1081}$
cHCV#12	female	72	297000	nd	nd	naïve	1b	A*02:01	$NS3_{1073-1081}$
cHCV#13	male	54	1799994	68	111	Glecaprevir/Pibrentasvir	3a	A*02:01	$NS3_{1406-1415}$
cHCV#14	female	64	7332185	60	78	Ledipasvir/Sofosbuvir/Ribavirin	1a	A*02:01	$NS3_{1073-1081}$
cHCV#15	male	35	40256	nd	nd	Ombitasvir/Paritaprevir/Ritonavir/Dasabuvir	1b	A*02:01	$NS3_{1073-1081}$
cHCV#16	female	78	189675	56	64	Glecaprevir/Pibrentasvir	1b	A*02:01	$NS3_{1073-1081}$
cHCV#17	female	65	571421	123	199	Sofosbuvir/Ribavirin	2a	A*02 pos.	$NS5B_{2841-2849}$
cHCV#18	female	35	54244	52	64	Ledipasvir/Sofosbuvir	1b	A*02 pos.	$NS3_{1073-1081}$
cHCV#19	female	48	nd	21	23	naïve	1a	A*02:01	$NS3_{1406-1415}$, $NS5B_{2841-2849}$
cHCV#20	male	41	nd	40	42	Peginterferon/Ribavirin	1a	A*02 pos.	$NS3_{1073-1081}$
cHCV#21	male	55	4586011	41	54	Glecaprevir/Pibrentasvir	1	A*02:01	$NS3_{1073-1081}$, $NS3_{1406-1415}$
cHCV#22	female	27	41555	20	28	Sofosbuvir/Peginterferon/Ribavirin	1a	A*02:01	$NS3_{1073-1081}$
cHCV#23	male	32	70997	56	125	Glecaprevir/Pibrentasvir	3a	A*02:01	$NS3_{1073-1081}$
cHCV#24	female	43	123048	33	41	Peginterferon/Ribavirin	1b	A*02:01	$NS3_{1073-1081}$
cHCV#25	female	61	43842	23	22	naïve	1	A*02:01	$NS3_{1073-1081}$
cHCV#26	male	42	95067	43	88	Peginterferon/Ribavirin	1b	A*02:01	$NS3_{1073-1081}$
cHCV#27	male	39	1466614	51	61	naïve	1a	A*02:01	$NS5B_{2841-2849}$
cHCV#28	male	61	1393356	86	142	Peginterferon/Ribavirin/Boceprevir	1b	A*02:01	$NS3_{1073-1081}$
cHCV#29	male	62	159807	89	128	Peginterferon/Ribavirin	3a	A*02:01	$NS3_{1073-1081}$
cHCV#30	female	51	404833	37	51	naïve	1a	A*02 pos.	$NS3_{1073-1081}$
cHCV#31	male	43	337092	49	60	Sofosbuvir/Velpatasvir	3a	A*02 pos.	$NS5B_{2841-2849}$
cHCV#32	male	70	4726534	56	60	Ledipasvir/Sofosbuvir	1a	A*02 pos.	$NS3_{1073-1081}$
cHCV#33	female	54	2158598	85	57	Ledipasvir/Sofosbuvir	1a	A*02:01	$NS3_{1073-1081}$
cHCV#34	female	57	726936	75	103	Ledipasvir/Sofosbuvir	1b	A*02:01	$NS3_{1073-1081}$
cHCV#35	male	39	514053	114	247	Sofosbuvir/Velpatasvir	3a	A*02:01	$NS5B_{2841-2849}$
cHCV#36	male	44	123843	66	130	Ledipasvir/Sofosbuvir	1a	A*02:01	$NS3_{1073-1081}$
cHCV#37	male	56	3238495	46	45	Ledipasvir/Sofosbuvir	1a	A*02:01	$NS3_{1406-1415}$
cHCV#38	male	38	3288239	88	208	Elbasvir/Grazoprevir	1b	A*02:01	$NS3_{1073-1081}$
cHCV#39	male	46	2325161	42	83	Ledipasvir/Sofosbuvir	1a	A*02:01	$NS3_{1073-1081}$
cHCV#40	male	54	4905790	48	47	Glecaprevir/Pibrentasvir	2b	A*02:01	$NS3_{1073-1081}$
cHCV#41	female	58	620160	47	63	Elbasvir/Grazoprevir	1b	A*02:01	$NS3_{1073-1081}$
cHCV#42	male	54	2030000	107	151	Ledipasvir/Sofosbuvir	1a	A*02:01	$NS5B_{2841-2849}$
cHCV#43	male	32	1123852	48	67	Ledipasvir/Sofosbuvir	1a	A*02:01	$NS3_{1406-1415}$
cHCV#44	male	53	479000	53	73	Ledipasvir/Sofosbuvir	1a	A*02 pos.	$NS3_{1073-1081}$
cHCV#45	male	50	1625676	31	48	Elbasvir/Grazoprevir	1b	A*02:01	$NS3_{1073-1081}$
cHCV#46	female	60	429137	34	44	Ombitasvir/Paritaprevir/Ritonavir/Dasabuvir	1b	A*02:01	$NS3_{1406-1415}$
cHCV#47	male	61	2930792	36	43	Glecaprevir/Pibrentasvir	1a	A*02:01	$NS3_{1406-1415}$
cHCV#48	male	55	2905593	36	49	Glecaprevir/Pibrentasvir	1a	A*02:01	$NS3_{1406-1415}$
cHCV#49	male	45	1952905	62	116	Glecaprevir/Pibrentasvir	1a	A*02:01	$NS3_{1073-1081}$
cHCV#50	female	53	207805	12	nd	Glecaprevir/Pibrentasvir	3a	A*02:01	$NS5B_{2841-2849}$
cHCV#51	female	22	2941144	80	94	Elbasvir/Grazoprevir	1a	A*02:01	$NS3_{1406-1415}$
cHCV#52	female	56	nd	nd	51	naïve	nd	A*02:01	$NS3_{1406-1415}$

*Therapy-naïve cHCV patients were used for all analyses except DAA-based studies (see figure 4).

Supplemental table 3: Antibodies for flow cytometric analysis

Antibody	Conjugate	Clone	Isotype	Dilution	Supplier	Cat no.
anti-CCR7	BUV395	3D12	Rat IgG2a, κ	1:200	BD	740267
anti-CD3	AlexaFluor700	SK7	Mouse IgG1, κ	1:33	BioLegend	344822
anti-CD8	APC	SK1	Mouse IgG1, κ	1:200	BD	345775
anti-CD8	BUV496	RPA-T8	Mouse IgG1, κ	1:100	BD	612942
anti-CD27	PE-Dazzle594	M-T271	Mouse IgG1, κ	1:200	BioLegend	356422
anti-CD28	APC-eFluor780	CD28.2	Mouse IgG1, κ	1:20	eBioscience	47-0289
anti-CD28	PE	B-T3	Mouse IgG2a, κ	1:33	Diaclone	854.222.010
anti-CD38	BV421	HIT2	Mouse IgG1, κ	1:50	BioLegend	303526
anti-CD39	BV650	TU66	Mouse IgG2b, κ	1:33	BD	563681
anti-CD45RA	BUV737	HI100	Mouse IgG2b, κ	1:800	BD	612846
anti-CD57	BV605	QA17A04	Mouse IgG1, κ	1:100	BioLegend	393304
anti-CD122	PE-Cy7	TU27	Mouse IgG1, κ	1:33	BioLegend	339014
anti-CD127	BV510	HIL-7R-M21	Mouse IgG1, κ	1:100	BD	563086
anti-CD127	BV711	HIL-7R-M21	Mouse IgG1, κ	1:20	BD	563165
anti-ENO1	AlexaFluor488	EPR10863(B)	Rabbit IgG	1:200	abcam	ab205871
anti-IFN-γ	FITC	25723.11	Mouse IgG2b, κ	1:8.33	BD	340449
anti-PD-1	BV421	EH12.2H7	Mouse IgG1, κ	1:50	Biolegend	329920
anti-PD-1	BV786	EH12.1	Mouse IgG1, κ	1:33	BD	563789
anti-TIGIT	PerCP-eF710	MBSA43	Mouse IgG1, κ	1:50	eBioscience	46-9500
anti-TNF-α	PE-Cy7	MAb11	Mouse IgG1, κ	1:100	BioLegend	502930

Supplemental figure 1 (related to figure 2)

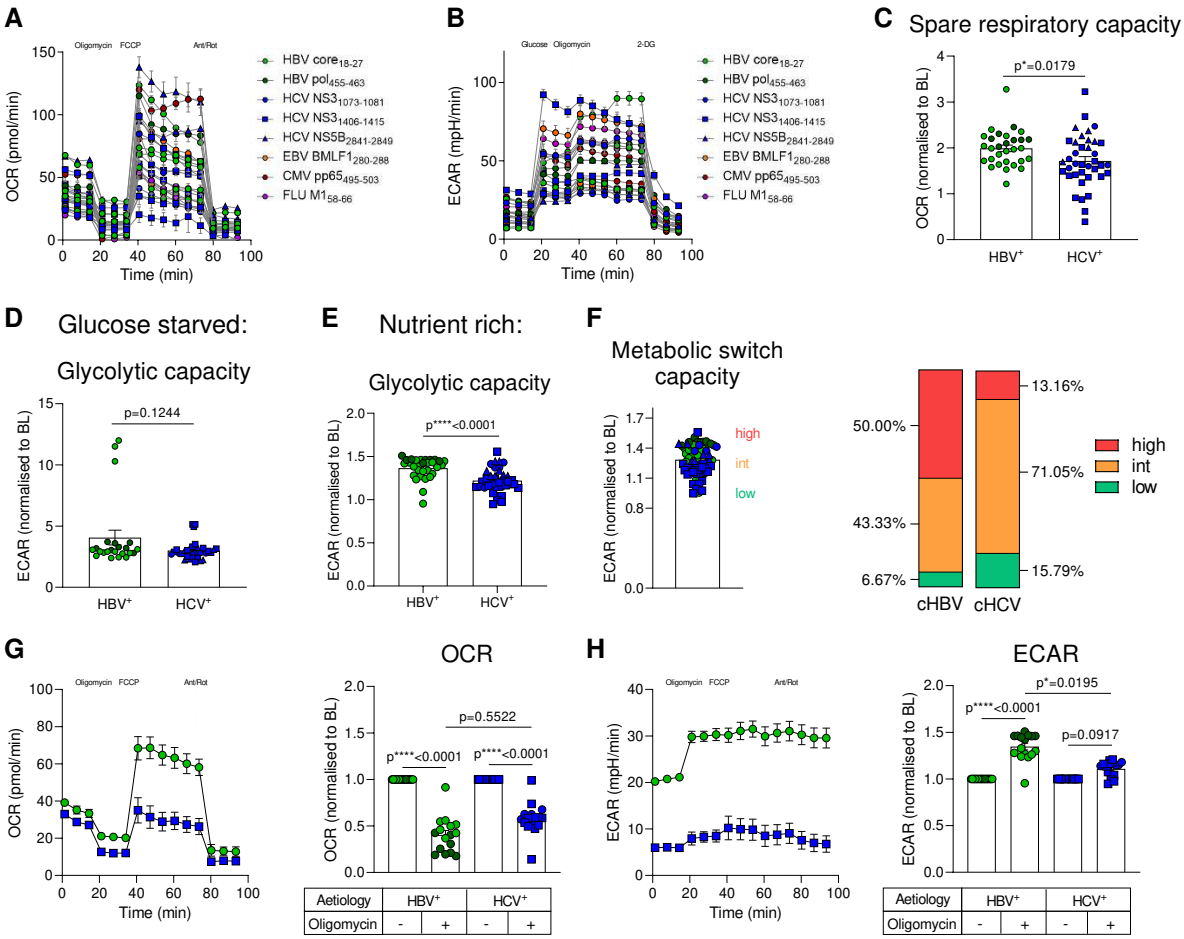

Supplemental figure 2 (related to figure 2)

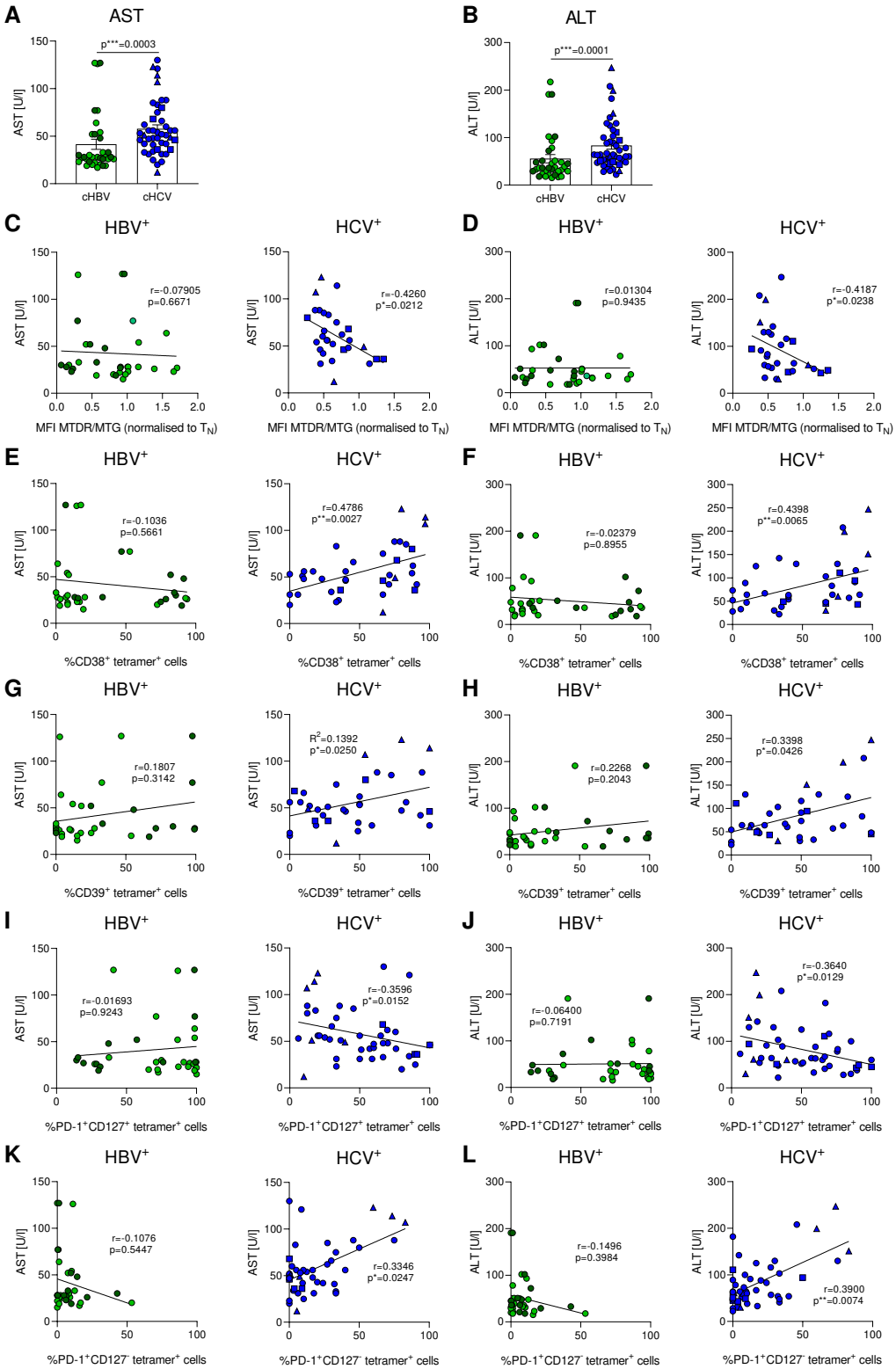

Supplemental figure 3 (related to figure 2)

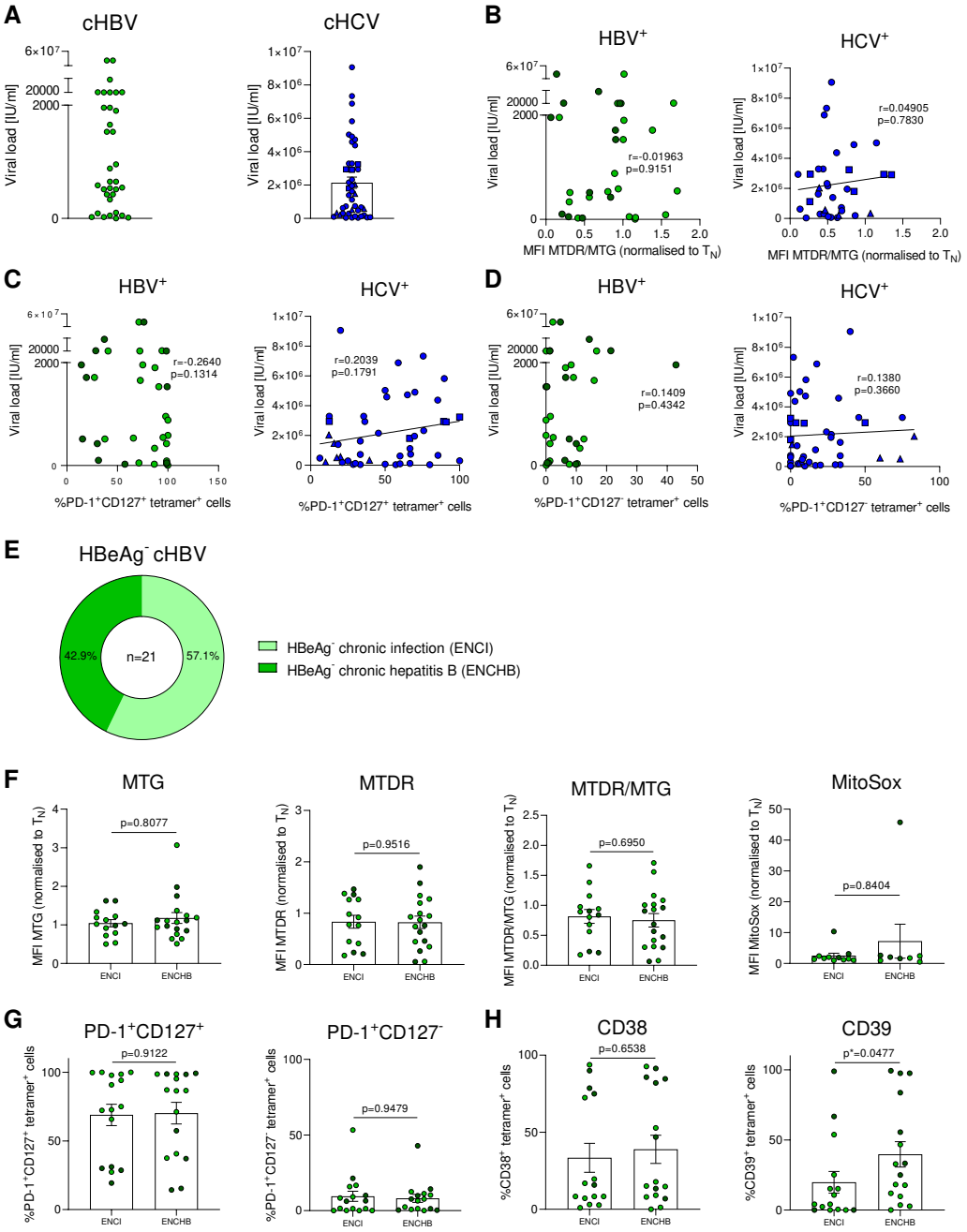

Supplemental figure 4 (related to figure 6)

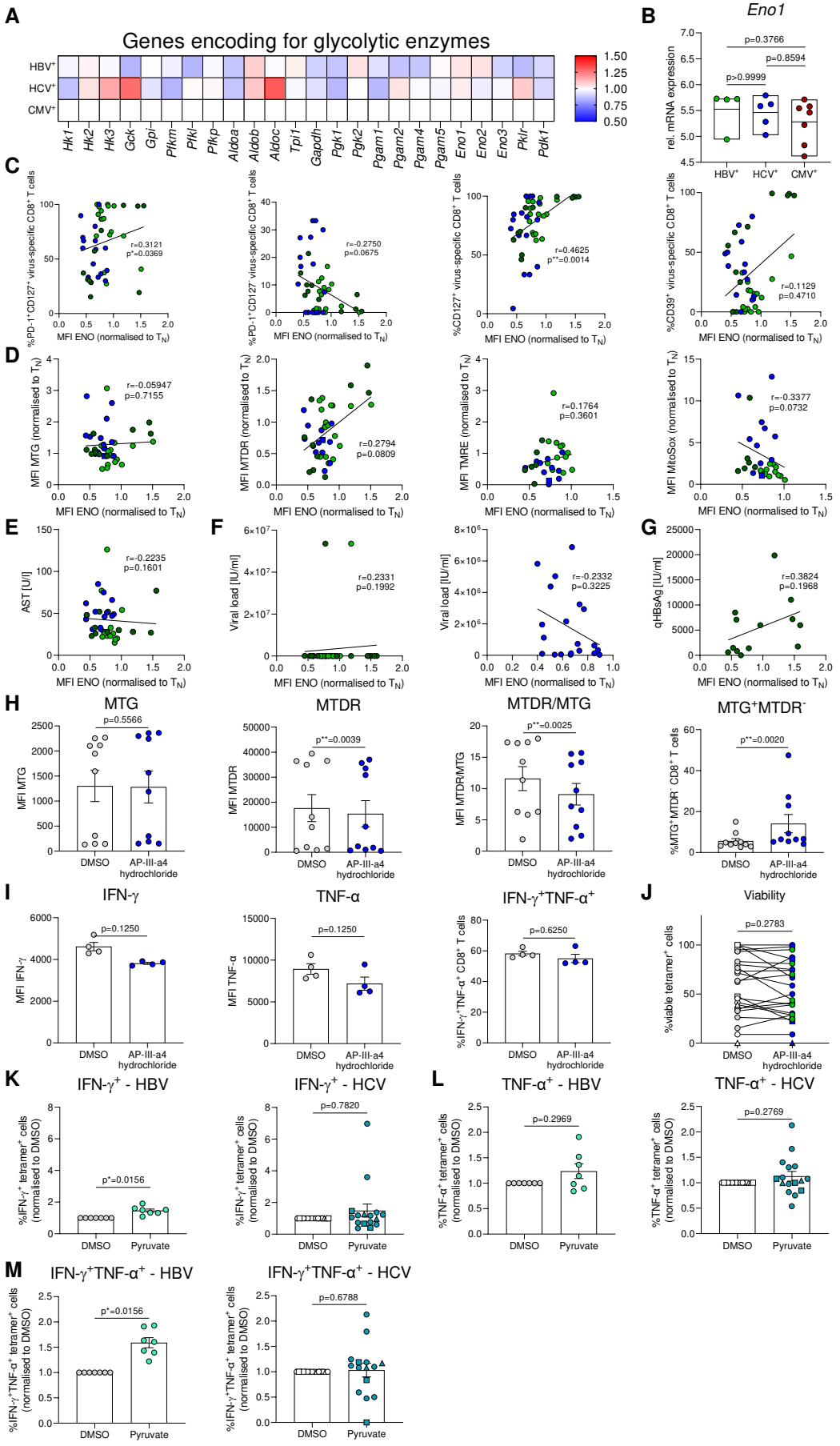

Supplemental figure 5 (related to figure 6)

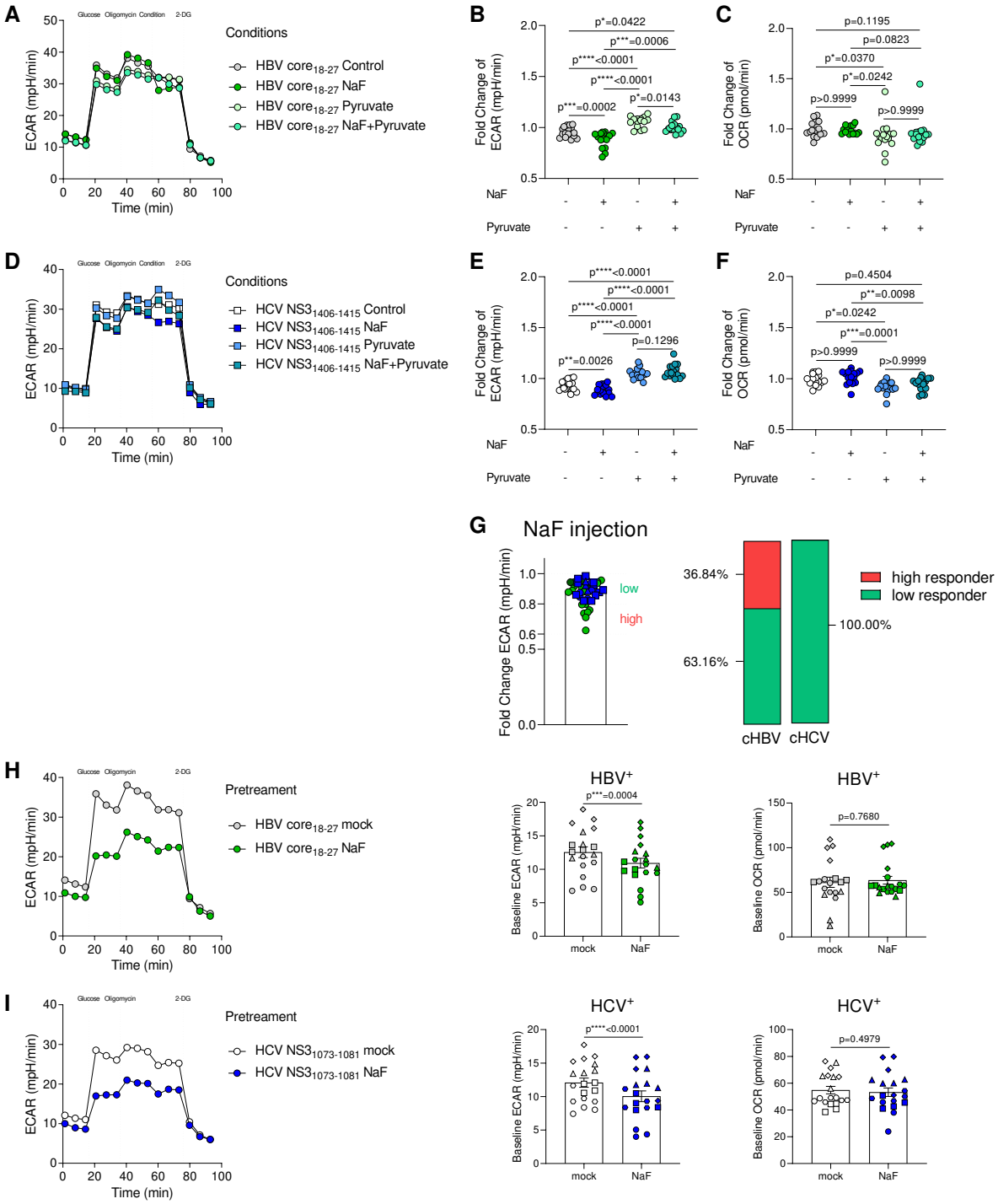

Supplemental figure legends

Supplemental figure 1. *In vitro* expanded HCV-specific CD8⁺ T cells exhibit diminished spare respiratory capacity and reduced metabolic switch capacity. Seahorse analysis: Quadruplicates of 200 000 expanded HBV- and HCV-specific CD8⁺ T cells were stimulated with cognate peptide and analysed for oxygen consumption rate (OCR) and extracellular acidification rate (ECAR). **(A)** Mito Stress Test was performed with time-delayed injections of oligomycin (1µM), FCCP (1.5µM), antimycin (1µM) and rotenone (0.1µM). **(B)** In the Glyco Stress Test *in vitro* expanded hepatitis virus-specific CD8⁺ T cells were exposed to subsequent injections of glucose (10mM), oligomycin (1µM) and 2-DG (50mM). **(C)** Spare respiratory capacity was determined in Mito Stress test experiments as the ratio of maximal respiration (after FCCP injection) to basal respiration. **(D)** Glycolytic capacity was determined in glucose-starved (Glyco Stress test) and **(E)** nutrient-rich (Mito Stress test) conditions as the ratio of maximal acidification rates (after oligomycin injection) to basal acidification rates. **(F)** ECAR after complex V inhibition by oligomycin are shown. Metabolic switch capacities of expanded HBV- and HCV-specific CD8⁺ T cells were categorised in low, intermediate and high and proportions are visualised. **(G)** OCR and **(H)** ECAR of expanded hepatitis virus-specific CD8⁺ T cells after oligomycin injection. To ensure appropriate comparison of different batches of expanded virus-specific CD8⁺ T cells, OCR and ECAR values were normalised to baseline for calculation of spare respiratory capacity and glycolytic capacity. Mann-Whitney test was performed in **(C-E)**. Kruskal-Wallis test was performed in **(G-H)**. Significance is indicated ($p^*<0.05$, $p^{****}<0.001$). Error bars indicate mean ±SEM.

Supplemental figure 2. Transaminase levels inform exhaustion severity and mitochondrial function of HCV-specific CD8⁺ T cells. (A-B) Transaminase activity (AST, aspartate aminotransferase; ALT, alanine aminotransferase) was assessed in serum of therapy-naïve cHBV and cHCV patients. **(C-D)** Correlation analyses of AST/ALT levels and mitochondrial polarisation (MTDR/MTG), **(E-F)** frequencies of CD38⁺, **(G-H)** CD39⁺, **(I-J)** PD-1⁺CD127⁺ and **(K-L)** PD-1⁺CD127⁻ virus-specific CD8⁺ T cells. HBV $core_{18-27}$ (green) and HCV $NS3_{1073-1081}$ epitopes (blue) are represented by circles. HCV $NS3_{1406-1415}$ and HCV $NS5B_{2594-2602}$ epitopes are visualized by blue squares and triangles, respectively. Mann-Whitney test was performed in **(A-B)**. Spearman r correlation analyses were performed in **(C-F)**, **(G**, left**)** and **(H-L)**. Pearson r correlation analyses were performed in **(G**, right**)**. Significance is indicated ($p^*<0.05$, $p^{**}<0.01$, $p^{***}<0.005$). Error bars indicate mean ±SEM.

Supplemental figure 3. HBV-specific CD8⁺ T cells of HBeAg-negative chronic hepatitis B (ENCHB) patients show increased CD39 expression. (A) Viral loads were determined in therapy-naïve cHBV and cHCV patients by using clinical tests. **(B)** Correlation analyses of

patients' viral loads and mitochondrial polarisation (MTDR/MTG) and **(C)** frequencies of PD-1$^+$CD127$^+$ and **(D)** PD-1$^+$CD127$^-$ subsets of HBV- and HCV-specific CD8$^+$ T cells. **(E)** Serum transaminase level of therapy-naïve HBeAg-negative cHBV patients and **(F)** their categorisation into HBeAg-negative chronic infection (ENCI) and HBeAg-negative chronic hepatitis B (ENCHB) patients. **(G)** Metabolic *ex vivo* staining of HBV-specific CD8$^+$ T cells for mitochondrial mass (MTG), mitochondrial membrane potential (MTDR), mitochondrial polarisation (MTDR/MTG) and mitochondrial ROS (MitoSox) of ENCI and ENCHB patients. Signals of metabolic stainings were normalised to naïve (CCR7$^+$CD45RA$^+$) CD8$^+$ T cells. **(H)** Frequencies of PD-1$^+$CD127$^+$, PD-1$^+$CD127$^-$, **(I)** CD38$^+$ and CD39$^+$ HBV-specific CD8$^+$ T cells in ENCI and ENCHB patients. Patients were classified as ENCI if AST and ALT level were normal and considered ENCHB if either their AST and/ or ALT activity was above the normal range of 10-35 U/l in females and 10-50 U/l in males. HBV core$_{18\text{-}27}$ (green) and HCV NS3$_{1073\text{-}1081}$ epitopes (blue) are represented by circles. HCV NS3$_{1406\text{-}1415}$ and HCV NS5B$_{2594\text{-}2602}$ epitopes are visualised by blue squares and triangles, respectively. Mann-Whitney test was performed in **(E)**, **(G**, MTG and MitoSox**)**, **(H**, right**)** and **(I)**. Unpaired t-test was performed in **(G**, MTDR and MTDR/MTG**)** and **(H**, left**)**. Spearman r correlation analyses were performed in **(B-D)**. Significance is indicated (p*<0.05, p**<0.01, p***<0.005). Error bars indicate mean ±SEM.

Supplemental figure 4. Enolase inhibition induced by AP-III-a4 hydrochloride negatively affects mitochondrial function of CD8$^+$ T cells from healthy individuals. (A) Heat map illustrating mRNA expression levels of genes encoding for key enzymes in the glycolytic pathway of therapy-naïve sorted HBV- (n=4) and HCV-specific CD8$^+$ T cells (n=5) normalised to sorted CMV-specific CD8$^+$ T cells (n=7). **(B)** Relative Eno1 mRNA expression of HBV- and HCV-specific CD8$^+$ T cells. **(C)** Correlation analyses of ENO1 expression and frequencies of PD-1$^+$CD127$^+$, PD-1$^+$CD127$^-$, CD127$^+$ and CD39$^+$ hepatitis virus-specific CD8$^+$ T cells **(D)** Correlation analyses of ENO1 expression and mitochondrial mass (MTG), mitochondrial membrane potential (MTDR, TMRE), mitochondrial ROS (MitoSox) and **(E)** serum AST level, **(F)** viral loads of therapy-naïve cHBV and cHCV patients and **(G)** HBsAg of cHBV patients. **(H)** Metabolic *ex vivo* staining of CD8$^+$ T cells isolated from healthy individuals for mitochondrial mass (MTG), mitochondrial membrane potential (MTDR), mitochondrial polarisation (MTDR/MTG) and the frequency of depolarised (MTG$^+$MTDR$^-$) mitochondria after o/n treatment with AP-III-a4 hydrochloride. **(I)** IFN-γ and TNF-α production of PMA- and ionomycin-stimulated CD8$^+$ T cells of healthy donors after o/n incubation with AP-III-a4 hydrochloride. **(J)** Frequencies of viable hepatitis virus-specific CD8$^+$ T cells after o/n exposure to AP-III-a4 hydrochloride. HBV core$_{18\text{-}27}$ (green) and HCV NS3$_{1073\text{-}1081}$ epitopes (blue) are represented by circles. HCV NS3$_{1406\text{-}1415}$ and HCV NS5B$_{2594\text{-}2602}$ epitopes are visualised by blue squares and

triangles, respectively. Kruskal-Wallis test was performed in **(B)**. Spearman r correlation analyses were performed in **(C-G)**. Wilcoxon test was performed in **(H**, MTG, MTDR and MTG^+MTDR^-**)**, **(I)** and **(K-M)**. Paired t-test was performed in **(H**, MTDR/MTG**)** and **(J)**. Significance is indicated (p*<0.05, p**<0.01). Error bars indicate mean ±SEM.

Supplemental figure 5. Enolase represents a metabolic checkpoint restricting the glycolytic flux in hepatitis virus-specific $CD8^+$ T cells. (A-F) Glyco Stress test was performed using quadruplicates of 200 000 expanded HBV- and HCV-specific $CD8^+$ T cells stimulated with cognate peptide and analysed for oxygen consumption rate (OCR) and extracellular acidification rate (ECAR). To this end, cells received time-delayed injections of glucose (10mM), oligomycin (1µM), sodium fluoride (NaF, 2mM) and/ or sodium pyruvate (2mM) and 2-DG (50mM). **(G)** ECAR values of HBV-and HCV-specific $CD8^+$ T cells after NaF injection were discriminated in high and low responders according to their ECAR drop after NaF injection. Frequencies of high and low NaF responders are illustrated. **(H-I)** Expanded hepatitis virus-specific $CD8^+$ T cells were exposed to sodium fluoride (2mM) 2h before measurement and basal ECAR and OCR levels were compared to mock-treated HBV- and HCV-specific $CD8^+$ T cells. One-way ANOVA was performed in **(B)** and **(E)**. Friedman test was performed in **(C)** and **(F)**. Paired t-test was performed in **(H**, left**)** and **(I)**. Wilcoxon test was performed in **(H**, right**)**. Significance is indicated (p*<0.05, p**<0.01, p***<0.005, p****<0.001). Error bars indicate mean ±SEM.

Supplemental methods

PBMC isolation

Peripheral blood from therapy-naïve chronically infected hepatitis B- and C patients was collected in EDTA-anticoagulated tubes at the University Medical Center Freiburg, Germany. Venous blood was transferred onto a lymphocyte separation medium gradient (Pancoll, PanBiontech GmBH) following peripheral blood mononuclear cell (PBMC) isolation that have been resuspended in freezing medium containing 80% fetal calf serum (FCS), 10% dimethyl sulfoxide and 10% RPMI1640 and were stored at -80°C until the day of experiment.

Multi-parametric flow cytometry

Prior to staining, PBMCs were thawed in RPMI1640 supplemented with 10% fetal calf serum, 1% penicillin/streptomycin, 1.5% 1M Hepes buffer containing 50U/mL benzonase (Sigma). Staining with a fixable viability dye (APC-eFluor780, 1:200, eBioscience; eFluor506, 1:100, eBioscience) was performed for 5 minutes at RT, followed by a tetramer staining for 15 minutes at RT. Metabolic staining was performed in complete RPMI medium for 20 minutes at 37°C and 5% CO_2. To detect glucose uptake, cells were incubated with the fluorescent glucose analogue 2-[N-(7-nitrobenz-2-oxa-1,3-diazol-4-yl) amino]-2-deoxy-D-glucose (2-NBDG, Thermo Fisher, 200µM). Several metabolic dyes were used to identify different complementary mitochondrial features. Mitochondrial mass was assessed using the MitoTracker Green probe (MTG, Thermo Fisher, 50µM). The mitochondrial mass and potential dependent fluorescent dye MitoTracker Deep Red (MTDR, Thermo Fisher, 10µM) was used in combination with MTG to distinguish polarised from depolarised mitochondria. In addition, the mitochondrial membrane potential was determined by staining with tetramethylrhodamine ethyl ester (TMRE, Biomol, 10nM), which accumulates in mitochondria in inverse proportion to the mitochondrial membrane potential according to the Nernst equation. Mitochondrial superoxides were analysed by exposing of PBMCs to MitoSox Red (MitoSox, Thermo Fisher, 5µM). In a next step, surface staining was performed for 10 minutes at 37°C, 5% CO_2 and 20 minutes at RT. After surface staining, PBMCs were resuspended in PBS containing 1% FCS and protected from light until analysis using FACSCanto II, LSRFortessa with FACSDiva software version 10.6.2 (BD) or CytoFLEX (Beckman Coulter) with CytExpert software version 2.3.0.84. Flow cytometric data were analysed using FlowJo software version 10.6.2 (Treestar). Metabolic stainings were analysed after normalisation of MFI signals to naïve $CD8^+$ T cells from the respective sample (defined as $CCR7^+CD45RA^+$) to address batch variation in metabolic data (**figure 2C**). For the detection of intracellular molecules, the FoxP3/transcription factor staining buffer set (Thermo Fisher) was used according to the

manufacturer's protocol. For sufficient detection of cytokines, PBMCs were stimulated prior to staining with phorbol-12-myristat-13-acetate (PMA, Sigma) and ionomycin (Sigma) in the presence of brefeldin A and monensin (BD) for 5 hours at 37°C and 5% CO_2. After intracellular cytokine staining, PBMCs were fixed in 2% paraformaldehyde (PFA). Antibodies used for flow cytometry are listed in **Supplemental table 3**.

Cell sorting

Freshly isolated PBMCs obtained from chronically HBV- and HCV-infected patients were stained with a fixable viability dye for 5 minutes at RT, the respective tetramer for 15 minutes at RT and a CD8 antibody for 15 minutes at RT, followed by single cell sorting of viable, tetramer$^+$ CD8$^+$ T cells into the sterile 96-well plate with allogenic feeder cells. Cell sorting for the generation of expanded HBV- and HCV-specific CD8$^+$ T cells was performed using the FACSMelody cell sorter (BD).

Microarray analysis

Virus-specific CD8$^+$ T cells from therapy-naïve patients with chronic hepatitis B virus (cHBV) and chronic hepatitis C virus (cHCV) infection and from CMV-positive healthy individuals were identified by flow cytometric staining with HLA-A*02:01-restricted tetramers directed against the following epitopes: HBV core$_{18\text{-}27}$: FLPSDFFPSV (n=4), HCV NS3$_{1073\text{-}1081}$: CINGVCWTV (n=4), HCV NS3$_{1406\text{-}1415}$: KLVALGINAV (n=1) and CMV pp65$_{495\text{-}503}$: NLVPMVATV (n=7). The yield of tetramer-specific CD8$^+$ T cells ranged from 220 to 15 000 cells. The RNeasy mini kit (Qiagen) was used to extract RNA from the flow cytometry sorted cells. Due to the low number of tetramer-positive cells, the RNA was amplified and converted to cDNA using the WT-OvationTM Pico RNA Amplification System (NuGEN, AC Leek, The Netherlands). The resulting single-stranded cDNA was fragmented, labelled using the Encore Biotin Module (NuGEN), and then hybridised to the Affymetrix® Human Genome U219 array plate in the GeneTitan® instrument (Affymetrix, Santa Clara, CA), according to the manufacturer's protocol. The Bioconductor package version 2.12 (working with R version 3.0.1) was used for microarray analysis. Probe annotation was performed using the alternative cdf version 17 based on Entrez Gene, assigning probes to 18 567 unique transcripts. Data pre-processing was performed using the RMA algorithm. Data from three different batches were combined, and a correction for batch effect was applied using the ComBat package. The data are deposited as GEO GSE60552.

Gene set enrichment analysis

Gene set enrichment analysis (GSEA) of metabolic pathways was performed on microarray data from sorted HBV- and HCV-specific $CD8^+$ T cells (deposited in GEO GSE60552) using the GSEA software (version GSEA v4.2.2). Gene sets from the Molecular Signature Database v.7.5.1 [1] including KEGG pathway gene lists obtained from http://www.genome.jp/kegg/pathway.html were used. In addition, the following exhaustion-related gene sets were used: (a) exhaustion (chronic $TCF1^-$), exhaustion memory-like (chronic $TCF1^+$), memory signature [2] and (b) genes up- and downregulated in exhaustion [3]. Normalised enrichment scores (NES) obtained by GSEA were used to compare different pathways of HBV- and HCV-specific $CD8^+$ T cells.

T cell expansion *in vitro*

PBMCs isolated from peripheral blood of HLA-A*02:01-positive cHBV and cHCV patients and healthy donors were stained with HLA-A*02:01-restricted fluorochrome-labelled peptide MHC-I tetramers, viability dye and surface antibodies (CCR7, CD45RA, CD8). In a next step, non-naïve, tetramer$^+$$CD8^+$ T cells were sorted into a sterile 96-well plate containing 100 µL medium and 200 000 allogeneic feeder cells derived from healthy donors (previously irradiated at 30 Gy for 30 minutes). Sorted single cells were supplemented with 40µg/mL phytohaemagglutinin (PHA) and incubated at 5% CO_2 and 37°C. Every 3-4 days, antigen-specific cells were supplemented with fresh medium (RPMI 1640 containing 10% human serum, 2mM L-glutamine, 100U/mL penicillin and 100µg/mL streptomycin) and 20U/mL IL-2. After 14 days, antigen-specific $CD8^+$ T cells were incubated with freshly isolated allogeneic feeder cells, transferred to a 48-well plate and maintained under the above conditions. After 28 days, the cells were restimulated and transferred to a 24-well plate. After 35 days and visible cell proliferation, expanded $CD8^+$ T cells were flow cytometrically tested for maintenance of antigen specificity and frozen at -80°C until further use. For metabolic flux analysis, antigen-specific $CD8^+$ T cell cultures were thawed and restimulated with allogeneic feeder cells and IL-2 as described above. Every 3-4 days, antigen-specific $CD8^+$ T cells received fresh medium and were supplemented with IL-2. After 14 days, antigen-specific $CD8^+$ T cells were restimulated with allogeneic feeder cells and IL-2. After 21 days, antigen-specific $CD8^+$ T cells were tested for antigen specificity and counted. Quadruplicates of 200 000 expanded virus-specific $CD8^+$ T cells were seeded in a 96-well plate precoated with Cell-Tak (Thermo Fisher Scientific). In total, virus-specific $CD8^+$ T cells were cultured for 8 weeks prior to the Seahorse experiments.

Seahorse extracellular flux analysis

200 000 expanded virus-specific $CD8^+$ T cells were seeded in quadruplicates into a 96-well polystyrene Seahorse plate (Agilent) precoated with Cell-Tak (Thermo Fisher Scientific) and equilibrated for 1 hour at 37°C and 5% CO_2. After equilibration, virus-specific $CD8^+$ T cells were incubated with cognate peptide for 2 hours. Cells were assayed for extracellular acidification rate (mpH/min) and oxygen consumption rate (pmol/min) using the Seahorse XF Cell Mito Stress Test Kit (Agilent) and the Seahorse XF Glycolysis Stress Test Kit. During the Mito Stress Test, cells were exposed to injections of oligomycin (1µM), FCCP (1.5µM), antimycin (1µM) and rotenone (0.1µM). During the Glycolysis Stress Test, cells received injections of glucose (10mM), oligomycin (1µM) and 2-DG (50mM). In addition, *in vitro* expanded antigen-specific $CD8^+$ T cells were injected or pre-incubated with sodium fluoride (2µM) (NaF) (Merck) and/or sodium pyruvate (2mM).

Patient and Public involvement

It was not appropriate or possible to involve patients or the public in the design, or conduct, of our research. Dissemination of the results of this study will be by press release, Twitter and making publications accessible to patients in our outpatient hepatology clinic.

Adenoviral vector

The Ad-HBV-Luc vector developed and reported by Manske *et al*. was used [4].

Mice

C57Bl/6 mice were purchased from Charles River and Cor93 TCR transgenic mice (B6.Cg-Ptprca Pepcb Tg(TcraBC10,TcrbBC10)3Chi/J) were purchased from The Jackson Laboratory. Mice were housed under specific pathogen-free conditions in the central animal facility of the Technical University of Munich, according to the guidelines of the Federation of Laboratory Animal Science Association. Adult male mice (older than 6 weeks) were used in the experiments. Adenoviral vectors were intravenously (i.v.) injected in 100 µL of 0.9% sodium chloride solution. All animal experiments were authorised by permission of the Regierung von Oberbayern (AZ: ROB-55.2.2532.Vet_02-18-90).

Adoptive T cell transfer

Naïve $CD44^{-}CD8^{+}$ T cells were isolated from the spleen and lymph nodes of Cor93 TCR transgenic mice by negative magnetic bead separation (Miltenyi Biotec). Next, 10 000 CD45.1 T cells were intravenously injected into the tail vein in 100 µL PBS.

Isolation of liver-associated lymphocytes

The livers of sacrificed mice were perfused with PBS via the portal vein, finely chopped and passed through a sieve. Liver cells were washed in PBS and then incubated in Gey's balanced salt solution (PAN Biotech,) supplemented with 0.125 U/mg collagenase type 2 (Worthington Biochemical Corporation) for 10 min at 37 °C. After enzymatic digestion, lymphocytes were isolated by Percoll (GE Healthcare) gradient centrifugation. Briefly, cells were resuspended in a 40% Percoll solution and underlaid with an 80% Percoll solution. The isolated lymphocytes were washed in PBS and then used for cell sorting of $Cor93^{+}CD45.1^{+}CD8^{+}$ T cells.

scRNA-Seq preprocessing

ScRNA-Seq preparation was performed using the Chromium Next GEM Single Cell 3´ Kit V3.1 (10x Genomics, Pleasanton, California, US) according to the manufacturer's instructions. Sequencing was performed on a NovaSeq6000 Paired-End S1 Flowcell. scRNA-Seq bioinformatic analysis was performed in R version 4.0.2. The 10x cellranger sequencing pipeline and cell hashing were used to attenuate batch effects and followed the Seurat (4.0.5) vignette to demultiplex the counts information. Doublet cells (with more than one hashtag) were removed. For quality control, we removed cells with the following conditions: a number of UMI less than 300 or more than 30 000; above 5 000 features; mitochondrial reads greater than five percent. Counts were log normalised and scaled. For UMAP projection we used the following parameters n.neighbours = 350, min.dist = 0.01, and 50 dimensions in PCA in the RunUMAP Seurat function. Gene expression densities were visualised using Nebulosa V1.0.2. The glycolysis, TCA cycle and OXPHOS metabolic pathways were obtained from Xiao *et al.* [5]. Cells were scored using AUCell (V1.12.0). For the GSEA analysis we used the signatures of Bengsch *et al*. and Utzschneider *et al*. [2, 3].

Supplemental references

1 Subramanian A, Tamayo P, Mootha VK, Mukherjee S, Ebert BL, Gillette MA*, et al.* Gene set enrichment analysis: a knowledge-based approach for interpreting genome-wide expression profiles. Proc Natl Acad Sci U S A 2005;**102**:15545-50.

2 Utzschneider DT, Charmoy M, Chennupati V, Pousse L, Ferreira DP, Calderon-Copete S*, et al.* T Cell Factor 1-Expressing Memory-like CD8(+) T Cells Sustain the Immune Response to Chronic Viral Infections. Immunity 2016;**45**:415-27.

3 Bengsch B, Ohtani T, Khan O, Setty M, Manne S, O'Brien S*, et al.* Epigenomic-Guided Mass Cytometry Profiling Reveals Disease-Specific Features of Exhausted CD8 T Cells. Immunity 2018;**48**:1029-45 e5.

4 Manske K, Schneider A, Ko C, Knolle PA, Steiger K, Protzer U*, et al.* In Vivo Bioluminescence Imaging of HBV Replicating Hepatocytes Allows for the Monitoring of Anti-Viral Immunity. Viruses 2021;**13**.

5 Xiao Z, Dai Z, Locasale JW. Metabolic landscape of the tumor microenvironment at single cell resolution. Nature communications 2019;**10**:3763.

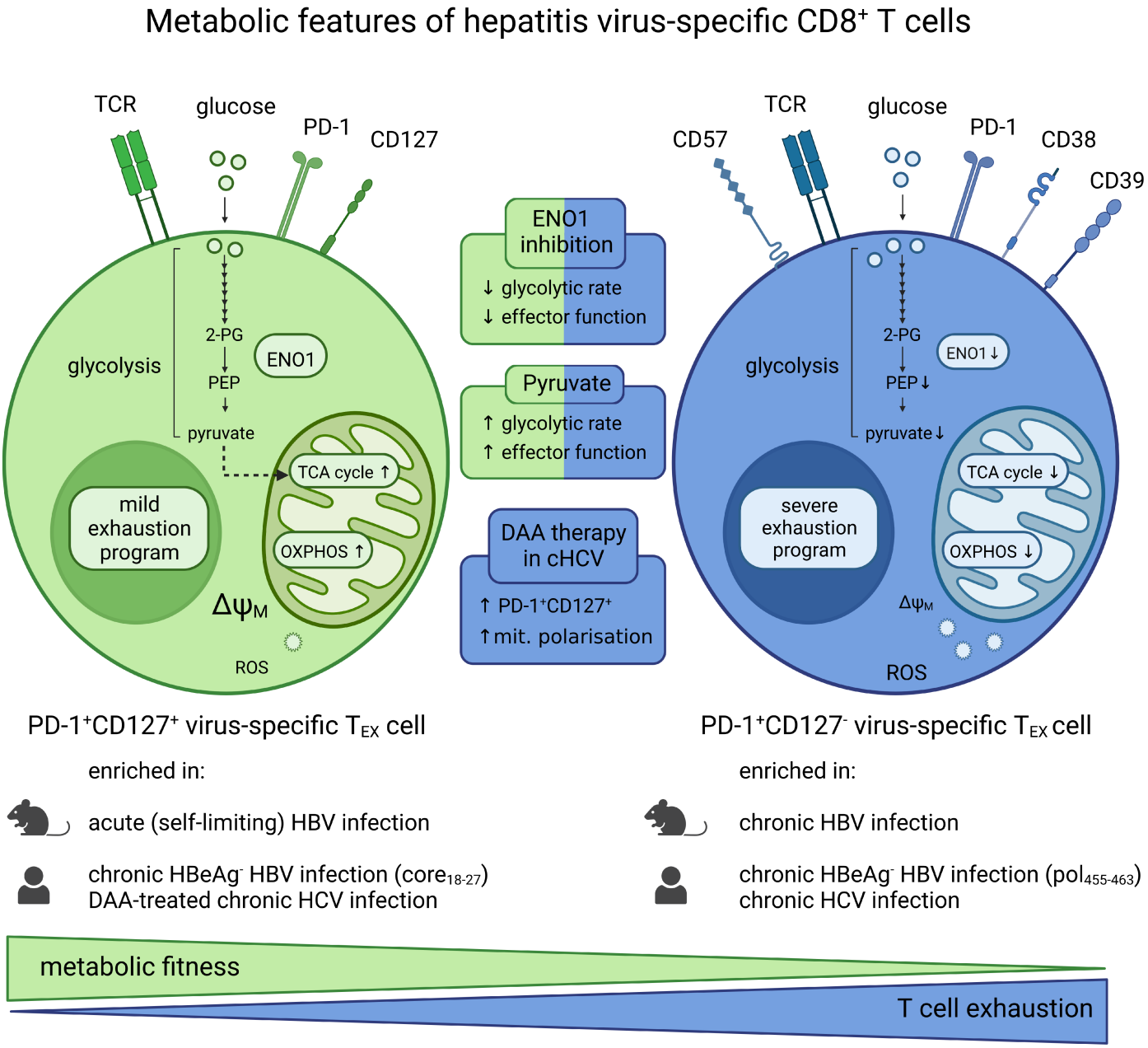
Metabolic features of hepatitis virus-specific CD8+ T cells
TCR
glucose
PD-1
CD127
glycolysis
2-PG
ENO1
PEP
pyruvate
TCA cycle ↑
mild exhaustion program
OXPHOS ↑
ΔψM
ROS
ENO1 inhibition
↓ glycolytic rate
↓ effector function
Pyruvate
↑ glycolytic rate
↑ effector function
DAA therapy in cHCV
↑ PD-1+CD127+
↑ mit. polarisation
TCR
glucose
PD-1
CD57
CD38
CD39
glycolysis
2-PG
ENO1 ↓
PEP ↓
pyruvate ↓
TCA cycle ↓
severe exhaustion program
OXPHOS ↓
ΔψM
ROS
PD-1+CD127+ virus-specific TEX cell
enriched in:
acute (self-limiting) HBV infection
chronic HBeAg- HBV infection (core18-27)
DAA-treated chronic HCV infection
PD-1+CD127- virus-specific TEX cell
enriched in:
chronic HBV infection
chronic HBeAg- HBV infection (pol455-463)
chronic HCV infection
metabolic fitness
T cell exhaustion